SCANNING PROBE MEASUREMENT SYSTEM FOR ROOM TEMPERATURE THERMOPOWER

By

Marvell Mukongolo

A THESIS

Submitted to
Michigan State University
in partial fulfillment of the requirements
for the degree of

MASTER OF SCIENCE

Electrical and Computer Engineering

2011

ABSTRACT

SCANNING PROBE MEASUREMENT SYSTEM FOR ROOM TEMPERATURE THERMOPOWER

By

Marvell Mukongolo

The development of new and established materials for use in thermoelectric devices, and the development of new measurement techniques for the advancement of research in the field are major initiatives of thermoelectrics research at Michigan State University. To achieve this, measurement systems created for this research have to be accurate and as well as diverse in their capabilities. A new measurement system with scanning probe capabilities has been developed to measure thermopower at room temperature. The degree of homogeneity of bulk thermoelectrical materials can be obtained with thermopower measurements due to the fact that the thermopower of a semiconductor is related to the concentration of impurities in the material. Devices made of inhomogeneous or segmented materials are known to have increased efficiency compared to devices with homogeneous composition. The ability to characterize in-homogeneity in devices adds a new dimension to the type of research that can be achieved. This thesis presents an introduction to the room temperature thermopower scanning probe. The system is designed to operate in an open air, room temperature environment. The system is fully automated with LabVIEW software used for control and data collection purposes. Reference materials were used to verify the systems accuracy. A study of segmented p-type materials composed of Bi_2Te_3-LASTT ($Ag(Pb_{1-x}Sn_x)_mSbTe_{2+m}$) and n-type materials composed of Bi_2Te_3-LAST ($AgPb_mSbTe_{2+m}$) is also be presented.

ACKNOWLEDGEMENTS

I would like to take this opportunity to thank Dr. Timothy Hogan, for his unwavering support, guidance and encouragement throughout the years I have had the opportunity to be his student. Being a part of his research group has given me valuable experience and has helped me reach greater heights in my pursuit of knowledge.

I would to thank Dr. Chun-I Wu and Dr. Jonathan D'Angelo, for their guidance and mentorship throughout my research. I will forever be grateful for the mentorship I received from these two gentlemen.

I would like to thank Dr. Donnie Reinhard and Dr. Virginia Ayres for taking the time to review my thesis and serve on my thesis committee.

I would like to thank Dr. Percy Pierre and Dr. Barbara O'Kelly for their guidance in helping me attend graduate school and their support while I was in graduate school.

Finally, I would like to thank my mother, brother and sister for providing me the necessary motivation to succeed in my endeavors.

TABLE OF CONTENTS

LIST OF TABLES

LIST OF FIGURES

Key to Symbols

Symbol	Discription
E_{av}	Average energy
S	Absolute Seebeck coefficient
k_B	Boltzmann's constant {1.38×10^{-23} (J/K) = 8.616×10^{-5} (eV/K)}
ζ	Chemical potential
ϕ	Coefficient of performance for cooling applications
n	Concentration of free electrons
p	Concentration of free holes
N	Density of states
η	Efficiency of a thermoelectric generator
σ	Electrical conductivity
σ_c	The electrical conductivities of carriers in the conduction band
σ_v	The electrical conductivities of carriers in the valence band
E	Electron energy
q	Elementary charge {1.602×10^{-19} C}
E_{FO}	Fermi energy at 0K
ZT	Figure of merit
U	Internal energy
L	Lorenz number
λ	Mean free path
τ_o	Mean scattering time
μ	Mobility
τ	Relaxation time
T	Temperature
κ	Thermal conductivity
τ_m	Thomson coefficient

Chapter 1: Introduction to Thermoelectrics

1.1 Introduction

Due to advancements in technology and a greater demand for energy by the global population, there has never been a greater need for complementary energy sources and alternatives to fossil fuel than there is today. There is an impending crisis looming due to the fact that more and more countries are becoming developed nations, while the world's supplies of developed energy sources are being depleted at an alarming rate. Considering the fact that the world's population is set to increase by three billion within a life time, the need to develop alternative sources to diversify the world's energy supply has never been greater. A larger population, higher demand and depleting resources will likely lead to social unrest in the near future if this crisis is not averted. The solution to this problem is very clear; efficient renewable energy sources have to be found in order to avoid a global energy crisis.

Since the discovery of the Seebeck effect in the early 19th century, thermoelectrics (TE) research has focused in part on using electric transport phenomena as a basis for energy production. For years, researchers studying TEs have searched for ways to efficiently use the advantages that solid state devices provide. These devices are silent, scalable and require no moving parts. It is important to note that thermoelectrics is not viewed as a solution to the dependence on fossil fuels, but with increased efficiency TEs can be a component in a wide range of alternative energy technologies designed to help meet the greater demand from energy, improve the efficiency of energy use, bring diversity to the world's energy supply, and reduce environmental pollution.

The Electronic Materials Characterization and Pulsed Laser Deposition Lab at Michigan State University is one group in a collaborative effort between the Electrical and Computer

Engineering, Chemical Engineering and Material Science, Chemistry, Mechanical Engineering, and Physics and Astronomy departments as well as other universities to develop new thermoelectric materials. At the same time new measuring techniques are being developed in the lab to further advance research in this field.

Greater understanding of TE materials requires various transport measurement techniques. As part of this research a new measurement system has been developed to measure thermopower (or absolute Seebeck coefficient) in an open air, room temperature environment. This system allows for scanning probe capabilities for greater characterization abilities. The thermopower of a semiconductor is related to the concentration of impurities, using this information an indication of the degree of homogeneity of a sample can be obtained by measuring the thermopower from point to point on the surface of a sample. Inhomogeneous TE devices have been known to increase the efficiency of these devices and this concept will be discussed in further detail in later chapters. This system can also help gain insight into doping effects near metal contacts.

Chapter 2: Thermoelectric Principles

2.1 Introduction

Thermoelectric devices can be used in cooling applications when electric energy is supplied to the device or in power generation applications when heat energy is supplied to the device. For cooling applications the coefficient of performance (ϕ) is defined as the heat flow into the cold side of the thermoelectric cooler over the electric power supplied to the device. For power generation the efficiency of the device (η) is defined as the electrical power output from the module over the heat flow into the hot side of the device. As a generator, thermoelectrics can utilize waste heat to help improve the efficiency of existing energy sources and help to minimize adverse environmental impact. TE devices, however, have not reached a level of development where they are efficient enough to replace mechanical electric generators or to compete with devices such as compressor based refrigerators. The quality of a thermoelectric material depends on the material properties of electrical conductivity (σ), thermal conductivity (κ), absolute Seebeck coefficient (S) and temperature (T) through a figure of merit, ZT. A higher ZT results in a higher efficiency material, and maximizing the figure of merit requires a large absolute Seebeck coefficient, high electrical conductivity, and low thermal conductivity. The equation for ZT is: [1]

$$ZT = \frac{\sigma S^2}{\kappa} \cdot T \tag{2.1}$$

For comparison, a freon based refrigerator has a coefficient of performance (ϕ) of 1.4[1]. To achieve this with a TE device operating near room temperature would require a ZT of 4-5 [2]. Bismuth telluride (Bi_2Te_3) is one of the oldest and best known TE materials, with a ZT of ~1 at

[1] Detailed explanation of Coefficient of Performance and Ideal efficiency in section 2.9

room temperature when properly doped and alloyed with Bi_2Se_3 (for n-type materials) or Sb_2Te_3 (for p-type materials). One can see the lengths researchers still have to go to find TE materials that can rival devices currently in use.

Maximizing the *ZT* of a sample requires knowledge of the transport characteristics of the material. To have a high thermopower a material should only have a single type of carrier (p-type or n-type), with a low carrier concentration. Unfortunately low carrier concentrations result in low electric conductivity [1]. Finding a balance between the three transport characteristics is one of the challenges facing researchers trying to optimize TE materials to achieve higher ZT values.

This chapter will give an in-depth explanation into the principles of thermoelectrics.

2.2 Seebeck Effect

In 1821, Thomas Seebeck discovered the first known thermoelectric phenomenon. The equation for the absolute Seebeck coefficient is simply

$$S = \frac{dV}{dT} (\mu V/K) \tag{2.2}$$

The sign of *S* represents the potential of the cold side with respect to the hot side. Both electrons and holes diffuse from the hot side to the cold side of the sample, thus n-type samples which have a majority of electrons yield negative thermopower voltage while p-type samples, having a majority of holes yield positive thermopower voltages. Figure 2.1 shows an example of this where a temperature gradient maintained across a homogeneous conductor without an external flow of current causes electrons to diffuse to the area with lower energy states (colder side). The accumulation of electrons on the cold side results in a voltage difference [4].

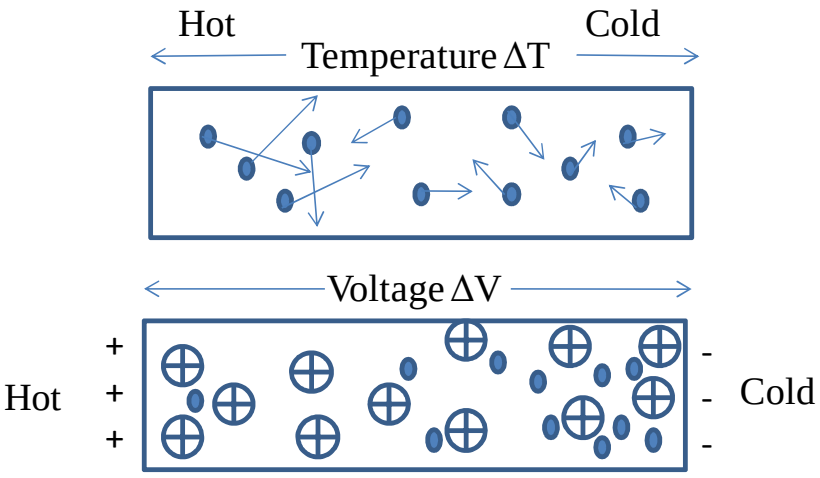

Figure 2.1: (For interpretation of the references to color in this and all other figures, the reader is referred to the electronic version of this thesis.)The absolute Seebeck Effect [4]

The potential difference ΔV across the conductor due to a temperature gradient ΔT is the thermopower (or absolute Seebeck coefficient) of the sample. The term Seebeck effect is applicable when there is a closed loop of two dissimilar materials with a presence of a temperature difference between the two junctions. The net Seebeck coefficient of the loop is considered to be the difference between the absolute Seebeck coefficients of the two materials that make up the loop [5].

2.2.2 Seebeck Effect in Insulators, Semiconductors, and Metals [5]

The Seebeck coefficient usually depends on carrier densities, the energy of states available to carriers, and the interactions of the carriers with one another and with the environment around them. These reasons make computations of the Seebeck coefficient very complex. One way the Seebeck coefficient can be derived is by considering an open circuit with no current flow. States occupied by charged carriers yield no net current when a system is in

thermal equilibrium. Thermal and potential gradients drive carriers to unoccupied states generating a net flow. This flow is opposed by scattering events which return the carriers to an equilibrium state. The relaxation time (τ) characterizes this re-equilibrium. The electric current density for an x directed flow influenced by an electric field $-\partial V/\partial x$ and temperature gradient $\partial T/\partial x$ is as follows:

$$J_n = \int dEN(E)f(E)[1-f(E)][v^2(E)\tau]\left[\left(\frac{-q}{k_BT}\frac{\partial V}{\partial x}\right)-\left(\frac{E-\zeta}{k_BT^2}\frac{\partial T}{\partial x}\right)\right]$$

$$= \int dE\sigma(E)\left[\left(-\frac{\partial V}{\partial x}\right)-\left(\frac{E-\zeta}{qT}\frac{\partial T}{\partial x}\right)\right] \quad (2.3)$$

Where $N(E)$ is the density of states, $v(E)$ is the carrier velocity, $f(E) = 1/\{\exp[(E-\zeta)/k_BT]+1\}$ is the Fermi distribution function for carriers of energy E and $\sigma(E)$ is the energy dependent electrical conductivity, q is the charge of the current carriers (-1.602×10^{-19} C for electrons), k_B is Boltzmann's constant and ζ is the chemical potential. From equation 2.3, the Seebeck coefficient can be obtained when there is an open circuit ($J_n = 0$).

$$\Delta V = \left(\frac{-1}{qT}\right)\frac{\int d(E)\sigma(E)[E-\zeta]}{\int d(E)\sigma(E)}\Delta T$$

$$\equiv \left(\frac{-1}{qT}\right)\langle[E-\zeta]\rangle_{\sigma(E)}\Delta T \quad (2.4)$$

Equation 2.4 shows the potential drop across a material in response to a temperature gradient. The Seebeck voltage ΔV is proportional to the average of $E-\zeta$ with respect to $\sigma(E)$, this is defined by $\langle[E-\zeta]\rangle_{\sigma(E)}$.

For insulators the Seebeck coefficient is usually greater than $k_B/|q|$=86μV/K ($|q|$ denotes the absolute value of the charge of an electron) and in some cases this can be as much as 1mV/K. Conversely in metals, the carrier density is a significant fraction of the density of thermally available states, which explains the low value of the Seebeck coefficient in electrical conductors (usually under 10μV/K). To have a better understanding of the reason behind this difference in Seebeck coefficients it is useful to rewrite equation 2.2 as

$$S = \left(\frac{k_B}{|q|}\right)\frac{\langle E-\zeta\rangle_{\sigma(E)}}{k_B T} \tag{2.5}$$

The entropy of a system of N carriers is $(U-\zeta N)/T$, U being the systems internal energy. Adding a carrier changes this to $(\Delta U-\zeta)/T$, $\Delta U=E$ is equal to the change in the systems internal energy. Without k_B, equation 2.3 can be described as "the average change of the entropy of a system upon the addition of a carrier of energy E weighted by that carrier's contribution to the dc conductivity divided by qT". With k_B in the formula, k_B/q appears as the natural unit with which to measure the Seebeck coefficients magnitude.

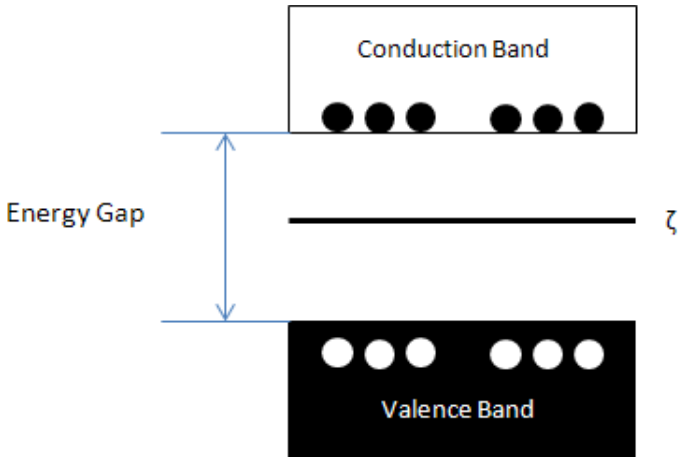

Figure 2.2: Ideal Insulator [5]

Illustrated in Figure 2.2 is an ideal intrinsic insulator with the chemical potential near the center of the energy gap between the valence and conduction bands. Most states in the valence band are filled and holes are the charge carriers that populate this band. Most states in the conduction band are empty, with electrons populating this band. The Seebeck coefficient can be written as a weighted average due to holes in the valence band and electrons in the conduction band the following way:

$$S = \frac{k_B}{|q|}\left[\left(\frac{\langle\zeta - E\rangle_V}{k_B T}\right)\left(\frac{\sigma_V}{\sigma_V+\sigma_C}\right) - \left(\frac{\langle E-\zeta\rangle_C}{k_B T}\right)\left(\frac{\sigma_C}{\sigma_C+\sigma_V}\right)\right] \quad (2.6)$$

where σ_V and σ_C represent the electrical conductivities of carriers in the valence and conduction bands respectively. Customarily the energies of valence and conduction band states are written relative to their respective band edges, E_C and E_V: $E = E_C - \varepsilon_C$ and $E = E_V - \varepsilon_V$. Equation 2.6 becomes

$$S = \frac{k_B}{|q|}\left[\left(\frac{\zeta - E_V}{k_B T} + A_V\right)\left(\frac{\sigma_V}{\sigma_V+\sigma_C}\right) - \left(\frac{E_C-\zeta}{k_B T} + A_C\right)\left(\frac{\sigma_C}{\sigma_C+\sigma_V}\right)\right] \quad (2.7)$$

where $A_V = \frac{\langle\varepsilon_V\rangle\sigma_V(E)}{k_B T}$ and $A_C = \frac{\langle\varepsilon_C\rangle\sigma_C(E)}{k_B T}$.

Most of the time one of the two terms inside the square brackets in equation 2.7 dominates the other. The Seebeck coefficient then becomes very large, $>> k_B/q$, since (ζ-E_V) and (E_C-ζ) are usually much larger than $k_B T$. At higher temperatures this Seebeck coefficient falls with increasing temperature in proportion to $1/k_B T$.

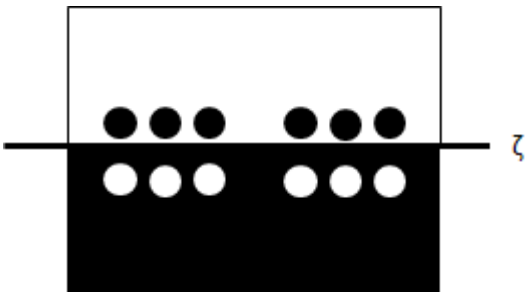

Figure 2.3: Metal [5]

Figure 2.3 shows the lack of a band gap in metals with the chemical potential of a metal residing within the band of states occupied by carriers. In this case the energy of the carriers can be expressed as $E = \zeta+\varepsilon$, where ε is the energy of the valence or conduction band states. For this particular case the product of the factors that involve Fermi functions, $f(E)[1-f(E)]$, in equation 2.4, can be approximated as a Gaussian function of ε that has peaked at about ε=0 with a width comparable to k_BT. The Seebeck coefficient for metals can then be represented as

$$S = \left(\frac{-1}{qT}\right)\frac{\int d\varepsilon N(\zeta+\varepsilon)\exp\left[-\left(\frac{\varepsilon}{2k_BT}\right)^2\right]v^2(\zeta+\varepsilon)\tau\varepsilon}{\int d\varepsilon N(\zeta+\varepsilon)\exp\left[-\left(\frac{\varepsilon}{2k_BT}\right)^2\right]v^2(\zeta+\varepsilon)\tau} \tag{2.8}$$

"Since the principle contribution of both integrals in equation 2.8 occurs at $\varepsilon < k_BT$, S must be small, $< k_B/|q|$." Evaluating equation 2.8 shows the Seebeck coefficient for metals vanishes at absolute zero, rises proportionally with temperature, and is very small.

$$|S| \approx \left(\frac{1}{|q|T}\right)\frac{\partial \ln\left[N(E)v^2(E)\right]}{\partial E}\Big|_{\zeta}(k_BT)^2$$

$$\approx \left(\frac{k_B}{|q|}\right)\left(\frac{k_B T}{\zeta}\right) \tag{2.9}$$

The typical chemical potential for metals is 1eV, while the value of $k_B T$ is usually 0.027eV, using equation 2.9, at 300K the Seebeck coefficient is only a few micro volts per Kelvin.

2.2.3 The Seebeck Effect and Metals [4]

For a metal with parabolic energy bands, the average energy, E_{av}, per electron is:

$$E_{av}(T) = \frac{3}{5} E_{FO}\left[1 + \frac{5\pi^2}{12}\left(\frac{k_B T}{E_{FO}}\right)^2\right] \tag{2.10}$$

where E_{FO} is the Fermi energy at 0 K. From this equation it can be seen that when the temperature is elevated, the average energy per electron also increases. This leads to the more energetic electrons on the hot end diffusing toward the cold region until a potential difference ΔV is built up which prevents further diffusion. For an electron to diffuse from the hot end to the cold end of a conductor the electron has to do work against the potential difference ΔV across that conductor which amounts to $q\Delta V$. This work decreases the average energy of the electron by ΔE_{av}, from E_{av}(hot) to E_{av}(cold):

$$q\Delta \mathrm{V} = E_{av}(T + \Delta T) - E_{av}(T)$$

Substituting equation 2.10 into E_{av} gives

$$\frac{3}{5} E_{FO}\left[1 + \frac{5\pi^2}{12}\left(\frac{k_B (T+\Delta T)}{E_{FO}}\right)^2\right] - \frac{3}{5} E_{FO}\left[1 + \frac{5\pi^2}{12}\left(\frac{k_B T}{E_{FO}}\right)^2\right]$$

Expanding ($T+\Delta T$), replacing ΔT with δT and neglecting δT^2 gives

$$q\delta V = \left[\frac{3}{5} E_{FO} \frac{5\pi^2}{12} \frac{{k_B}^2 2T\delta T}{{E_{FO}}^2}\right]$$

Finally using equation 2.2 the Seebeck coefficient of metals is,

$$S = \frac{\pi^2 {k_B}^2 T}{2qE_{FO}} \text{ (V/K)} \qquad (2.11)$$

It should be noted that this equation was derived with the assumption that the conduction electrons in the metal behave as if they were "free". Also the electron energy E = K.E. = $1/2 m_e^* v^2$ and the effective electron mass m_e^* are assumed to be constant with the velocity equal to the Fermi velocity. The final assumption is that higher energy electrons have greater mean speeds and longer mean free paths (λ) so they diffuse from the hot to cold ends of the conductors. These assumptions only apply to "normal" metals, such as aluminum, potassium, sodium, etc. Table 2-1 shows the Seebeck coefficients of various metals.

Table 2-1: Seebeck coefficients of various metals [4]

Metal	S at 0°C ($\mu V K^{-1}$)	S at 27°C ($\mu V K^{-1}$)
Na		-5
K		-12.5
Al	-1.6	-1.8
Mg	-1.3	
Pb	-1.15	-1.3
Pd	-9	-9.99
Pt	-4.45	-5.28
Mo	4.47	5.57
Li	14	
Cu	1.7	1.84
Ag	1.38	1.51

2.3 Peltier Effect [6]

Discovered by Jean Peltier in 1834, the Peltier Effect is a phenomenon in which heat is liberated or absorbed when an electric current passes through an in interface between two dissimilar conductors. The Peltier Effect is dependent on junctions between thermoelements where bulk materials are required for this phenomenon to take place.

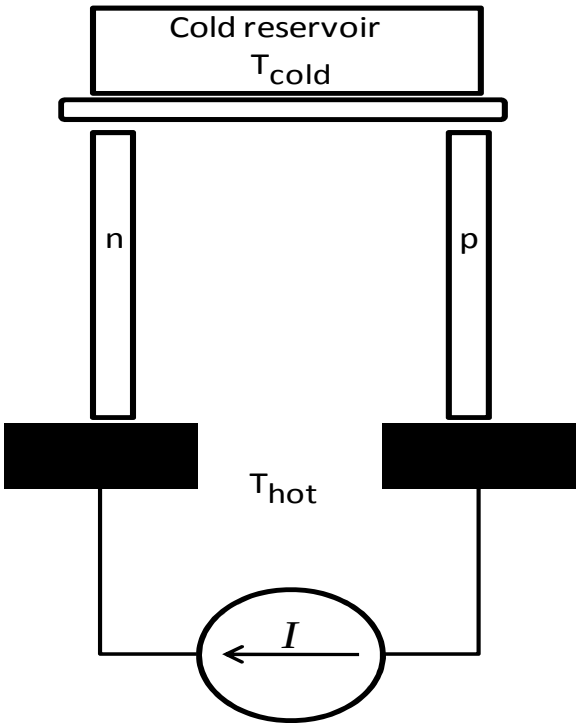

Figure 2.4: Peltier Effect [6]

The temperature rises or falls at the interface of the two dissimilar metals based on electric current going up or down a potential gradient. When the two metals are joined together there is a potential difference between them, known as the Peltier Coefficient, Π_{AB}. The amount of heat that is liberated or absorbed per unit time is proportional to the current applied; this relationship is given by the equation

$$Q = \Pi \cdot I \text{ (W)} \tag{2.13}$$

Since it is linearly dependent on current, heating or cooling at the junction is reversible by changing the current direction. In 1857 Lord Kelvin derived the relationship between the Seebeck and Peltier coefficients through a third effect called Thomson effect.

$$\Pi = T \cdot S \text{ (V/K)} \tag{2.14}$$

2.4 Thomson Effect [7]

The third of the thermoelectric phenomena is the Thomson Effect. Discovered in 1854 by the British physicist William Thomson later dubbed Lord Kelvin. He showed for current flowing in a homogeneous conductor along an imposed temperature gradient, a reversible process of heat production (or absorption) along the conductor exists. The Thomson Effect is characterized by the Thomson coefficient τ_m, which is very significant theoretically because it is used to complete the thermodynamic theory of thermoelectricity.

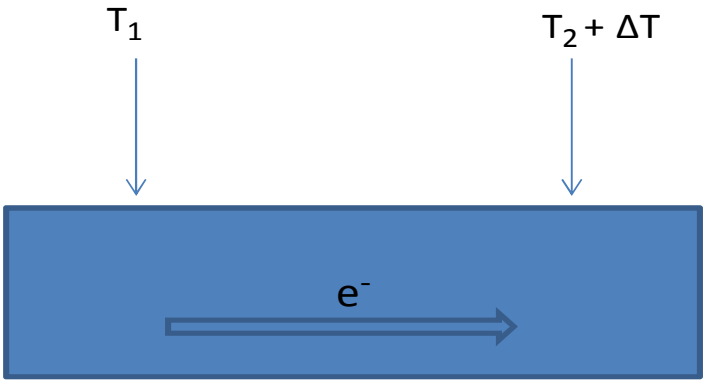

Figure 2.5: Thomson Effect [7]

The quantity of heat generated per unit time can be expressed as

$$dQ = (\tau_m I \frac{\mathrm{dT}}{\mathrm{dx}})\mathrm{dx} \tag{2.15}$$

where *dT/dx* is a temperature gradient along the homogeneous conductor carrying a current *I* in the *x*-direction with *dx* being a unit length. The direction of the current relative to the temperature gradient and the sign of τ_m determines whether heat is absorbed or liberated (i.e. if current flows in the direction in the direction of rising temperature and τ_m>0 then heat is liberated).

2.5 Electrical Conductivity[8]

In semiconductors charged particles (electrons and holes) move under the influence of electric fields. This movement creates drift current inside the semiconductor. The magnitude of the electrical conductivity is proportional to the density of the charge carriers in the material.

$$\begin{cases} J_{drift} = \sigma E_o \\ \sigma = q(\mu_n \cdot n + \mu_p \cdot p) \end{cases} \tag{2.16}$$

Where

σ = electrical conductivity (S/m)

E_o = electric field

n and *p* = carrier concentrations

μ = mobility

q= elementary charge (+1.602E-19)

2.6 Thermal conductivity [1]

Thermal conductivity is a measure of ability of a material to conduct heat. The total value of thermal conductivity κ takes into account the phonons traveling through the lattice

($\kappa_{Lattice}$) and electrons and holes transporting heat ($\kappa_{Electronic}$) can conduct heat through a material. Equation 2.17 shows this,

$$\kappa_{Total} = \kappa_{Electronic} + \kappa_{Lattice} \ (\mathrm{Wm^{-1}K^{-1}}) \tag{2.17}$$

The Wiedemann-Franz Law states that the ratio of the electronic contribution to κ and electrical conductivity (σ) of a metal is proportional to the temperature. This is shown in equation 2.18,

$$\frac{\kappa}{\sigma} = L \cdot T \ (\mathrm{W\Omega K^{-1}}) \tag{2.18}$$

where

κ= thermal conductivity (W/m·K)

σ = electrical conductivity (S/m)

L = Lorenz number = 2.45×10^{-8} ($\mathrm{W\Omega K^{-2}}$)

T = Temperature (K)

2.7 A Good Thermoelectric [9]

While doing research in thermoelectrics, one looks for materials with a figure of merit (*ZT*) near 1 or higher at some temperature. Materials used in power generation have their peak *ZT* values at high temperatures, while materials used in refrigiration have their peak *ZT* at low temperatures. High *ZT* materials typically have the following properties: low thermal conductivity ($\kappa_{Lattice}$= 0.5 – 1.0 W/m·K), high mobilities for the electrons and holes (μ > 1000 $\mathrm{cm^2/V \cdot s}$), at least four equivalent band minima (be multivalley), and posses a large density of states effective masses.

For applications near or at room temperature Bi_2Te_3 is the best known TE material. For p-type samples it is alloyed with Sb_2Te_3, and for n-type samples it is alloyed with Bi_2Se_3. Table 2-2 shows several Bi_2Te_3 based materials with comparable room temperature *ZT* values.

Table 2-2: Bi_2Te_3 alloys

Material	**ZT**	**Type**
$\mathbf{Bi_{24}Sb_{68}Te_{142}Se_6}$	0.96	p
$\mathbf{Bi_{0.5}Sb_{1.5}Te_{3.13}}$	0.9	p
$\mathbf{(Sb_2Te_3)_{72}(Bi_2Te_3)_{25}(Sb_2Se_3)_3}$	1.02	p
$\mathbf{Bi_{1.75}Sb_{0.25}Te_{3.13}}$	0.66	n
$\mathbf{(Sb_2Te_3)_5(Bi_2Te_3)_{90}(Sb_2Se_3)_5}$	0.96	n

(p-type and n-type materials can be formed with variations of the mole fraction of Te)

The structure of Bi_2Te_3 is stacked in a five-layer sequence (Te-Bi-Te-Bi-Te), with hexagonal symmetry. This sequence repeats so two Te layers are adjacent on the boundaries of these units. Bi_2Se_3, Sb_2Te_3, Bi_2Te_2Se, and other related compounds share this crystal structure. Other known attributes to Bi_2Te_3 are: both valence and conduction bands have six equivalent extrema, the energy bands are non parabolic and the effective masses are temperature dependent. Finally Bi_2Te_3 is usually alloyed with Sb_2Te_3 to reduce thermal conductivity causing an increase in its energy gap from 0.15 eV to 0.25 eV.

2.8 Thermocouples [10]

Thermocouples are commonly made of metals and utilize the Seebeck effect to measure the potential difference between two dissimilar metals, which in turn can be converted into a temperature. If there is a temperature gradient along the path of a wire, then there exists a potential across the wire. With dissimilar metals electrically joined at one end, the difference in the potentials across each wire is measured as the thermocouple voltage.

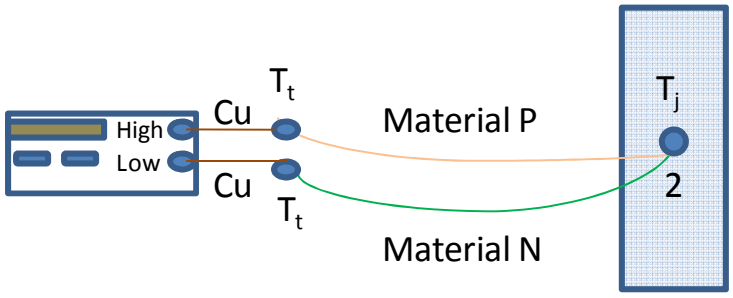

Figure 2.6: Thermocouple

The relationship between the Seebeck coefficient, ΔV and ΔT in thermocouples can be derived using equation 2.2. The ΔV due to the Seebeck effect is given by:

$$\Delta V = \int_{T_t}^{T_j} (S_P - S_N) dT = \int_{T_t}^{T_j} (S_{PN}) dT \tag{2.19}$$

Where T_t is the temperature at the voltmeter terminals and T_j is the temperature at the junction of the two dissimilar metals. As you can see from the above equation the net voltage (ΔV) of metals with equal Seebeck coefficients is zero. The relationship between the three components of equation (2.19) makes it possible to have various types of thermocouples, making it possible to use materials compatible with high or low temperature applications.

2.8.2 Reference Junctions

Thermocouples using two dissimilar wires only indicate temperature differences; in order to measure the absolute temperature a reference junction is required as shown in Figure 2.7 where T_r represents the temperature of the reference junction, and T_j is the thermocouple junction temperature.

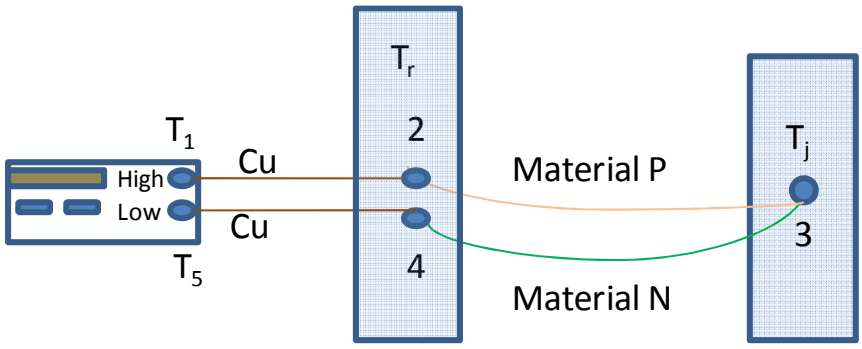

Figure 2.7: Thermocouple circuit with a reference junction

2.8.3 Ice Bath Reference

The National Institute of Standards and Technology (NIST) has developed tables for temperature values versus thermocouple voltage. This was done for a variety of standard thermocouples (Type: C, E, J, K, M, N, T). Using an ice bath (0 ºC) reference junction, reference tables have been generated for standard thermocouples.

Polynomial fits to the reference data are often used to conveniently convert between temperature and voltage for each thermocouple. To solve for voltage as a function of temperature the following polynomial curve fit is commonly used,

$$V_{0r} = F(T_r) = b_0 + b_1 T_r + b_2 T_r^2 + \ldots + b_n T_r^n \qquad (2.20)$$

For temperature as a function of voltage the following polynomial curve fit is used,

$$T_{0r} = G(V_{0r}) = c_0 + c_1 V_{0r} + c_2 V_{0r}^2 + \ldots + c_m V_{0r}^m \quad (2.21)$$

The coefficients for (2.20) and (2.21) are shown in Tables A-2 and A-3 of appendix A.

2.8.4 Practical Thermocouple Circuits

In a thermocouple circuit it may not be convenient to maintain an ice bath. Another method is to maintain the reference junction at an arbitrary, but known, temperature. This allows for the flexibility of only needing a simple temperature measurement device (i.e. resistance temperature detector (RTD) or temperature sensor diode) to find a reference temperature instead of devising a way to create an environment at 0°C (ice-bath).

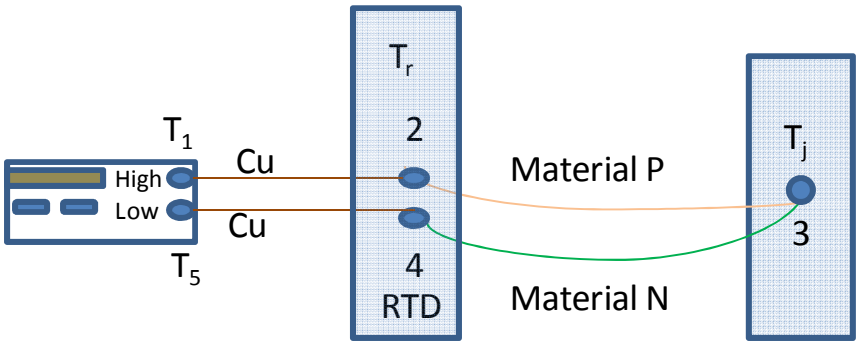

Figure 2.8: Thermocouple Circuit with RTD as reference.

To find the absolute temperature with a thermocouple using an arbitrary reference temperature, the value of the voltage at the terminals of the voltmeter and can be determined by integration as shown in equation (2.22).

$$V_{measured} = \int_{T_5}^{T_r} S_{Cu} \cdot dT + \int_{T_r}^{T_j} S_N \, dT + \int_{T_j}^{T_r} S_P dT + \int_{T_r}^{T_1} S_{Cu} \cdot dT \quad (2.22)$$

The first and fourth integrals in (2.22) account for the voltages developed by temperature gradients in the lead wires from the voltmeter. Since these wires have materials with the same thermopower (i.e. copper), it is assumed that the voltage developed is the same (i.e. $T_1 = T_5$) and the two integrals cancel each other. The next step is to determine the temperature at T_r by an independent method. Since $Tr \neq 0$ºC the standard thermocouple calibration data cannot be applied directly to equation (2.22). In this scenario let V_{rj} be the voltage generated between T_r and T_j, which is also the voltage shown in equation (2.22).

$$V_{rj} = \int_{T_r}^{T_j} S_{PN}\, dT \tag{2.23}$$

This can also be written as

$$V_{rj} = \int_{T_r}^{T_j} S_{PN}\, dT + \int_{0}^{T_r} S_{PN}\, dT - \int_{0}^{T_r} S_{PN}\, dT$$

$$= \int_{0}^{T_j} S_{PN}\, dT - \int_{0}^{T_r} S_{PN}\, dT$$

where

$$V_{0r} = \int_{0}^{T_r} (S_{PN}) dT \tag{2.24}$$

$$V_{0j} = \int_{0}^{T_j} (S_{PN}) dT \tag{2.25}$$

V_{0j} is the voltage of a thermocouple with T_r = 0°C and its measuring junction at T_j. V_{0r} is the voltage of a thermocouple with T_r= 0°C and its measuring junction at T_r. V_{rj} is measured by the

voltmeter, V_{0r} can be calculated by using the value of the temperature measured independently by an RTD, diode, or other temperature sensor in equation (2.20). Finally with these two values the V_{0j} can be calculated as

$$V_{0j} = V_{rj} + V_{or} \tag{2.26}$$

Using NIST data V_{0j} can be converted to a temperature using the following polynomial.

$$T_j = G(V_{oj}) = c_0 + c_1 V_{0j} + c_2 V_{0j}^2 + \ldots + c_m V_{0j}^m \tag{2.27}$$

2.9 Thermoelectric Devices

Thermoelectric devices are made of many couples wired electrically in series and thermally in parallel, consisting of n-type and p-type thermoelectric elements in pairs. Thermoelectric generators power externally connected electric loads, by converting the heat flow through the device into electricity. The heat flow acts as a driver of electric current and the temperature gradient provides the voltage ($V = S \cdot \Delta T$). At any given operating point, the product of the current and voltage determine the power output from the thermoelectric generator. Conversely, for Peltier coolers the power is supplied externally by a dc power supply. The power supply drives an external current (I) and heat flow (Q), thereby cooling the top surface due to the Peltier effect ($Q = S \cdot T \cdot I$). For both devices heat flow through the device must be maintained by appropriate heat exchangers [1]. The efficiency of a Peltier cooler can be quantified by the coefficient of performance (which is the net heat absorbed/applied electric power) [3]:

$$\Phi = \frac{Q_c}{I \cdot V} \tag{2.28}$$

where $I \cdot V$ is the electric power supplied to the module. The efficiency of a thermoelectric generator can be defined as the power delivered to a load resistance R by the heat supply Q which must be supplied to maintain a temperature gradient across the module [5].

$$\eta = \frac{I^2 R}{Q} \tag{2.29}$$

Impedance matching between the resistive load and the internal resistance of the thermoelectric generator is needed in order to have maximum power output.

\

Chapter 3: The Room Temperature Thermopower Scanning Probe

3.1 Introduction

In the Electronic Materials Transport Characterization and Pulsed Laser Deposition Laboratory, most of the measurement instruments are custom built with a specific goal in mind as far as performance is concerned. The main focus of TE research is to find ways to increase the *ZT* of materials as well as to identify new materials with promising properties for further research. It is important that data collected by our measurement systems is accurate and at the same time it is also important to the research that there is diversity in the capabilities of the measurement systems in the lab. Cross correlation of measurements of the same property taken on various systems helps to validate accuracy of the results. To build these systems one has to be knowledgeable of the governing principles behind thermoelectrics as well as posses skills in electrical and computer engineering. With these measurement systems the level of understanding of the transport characteristics of various TE materials can be achieved which leads to progressively better devices being produced. In this chapter the Room Temperature Thermopower Scanning Probe will be introduced. This chapter will provide detailed explanations about the design of the system.

3.2 History

Scanning probe microscopy is a method of microscopy in which an image is formed using a physical probe to scan the surface of a sample. An image of the surface of a sample is created by moving the probe over the surface of the sample and recording the probe to surface interaction as a function of position. This concept can also be applied when measuring thermopower. In some cases using multiple materials to create a TE sample can be advantageous when it comes to increasing the *ZT* of the sample.

The first systems of this kind were developed to "obtain an indication of the degree of homogeneity of a sample by the measuring of the variation of Seebeck coefficient from point to point" [11]. The apparatus by Cowles and Dauncey presented in 1962 showed a method of rapid scanning of the Seebeck coefficient of semiconductors. In their method a sample was placed on a metal heat sink, a heated probe was lowered on top of the sample creating a temperature gradient immediately below the probe. The temperature gradient was measured by two chromel-alumel thermocouples, one on the probe tip and the other inside the heat sink. The voltage across the sample was measured by the chromel wire. The ratio of the voltage across the sample to the difference between the voltages at the two thermocouples was determined directly. That ratio was equal to the Seebeck coefficients of the chromel-sample junction to the chromel-alumel thermocouples. Their circuit obtained this value using the ratio of an adjustable resistance to a fixed resistance, similar to a wheat stone bridge circuit. The heat sink was attached to a microscope stage whose slides permitted movement in the X-Y directions, while the probes movement was in the Z direction. There was no indication that these movements were motorized.

In 1986 Goldsmid [12] presented an improvement to Cowles and Dauncey's system by creating a simpler circuit requiring only a single balancing operation. Like the previous apparatus the probe and heat sink have the same design, the only difference being the thermocouple used in this case is a copper-constantan thermocouple. The voltage generated by the sample due to the temperature gradient is applied across three resisters (R_1, R_2, R_3) in series. The voltage generated at the junctions of the copper-constantan thermocouples is applied between one end of resistor R_1 and a null detector which is connected to the sliding contact of the potentiometer. The sliding contact is adjusted until the null detector indicates a balance bridge. If this balance is reached

when the resistance of the potentiometer winding is between the slider and the connection to R_1 is xR_2, then;

$$\frac{R_1 + xR_2}{R_1 + R_2 + R_3} = \frac{S_0 \Delta T}{S \Delta T} = \frac{S_0}{S}$$

ΔT being the temperature difference, S_0 is the Seebeck coefficient of the copper-constantan thermocouple and S is the required Seebeck coefficient of the semiconductor against copper. This technique is illustrated in Figure 3.1.

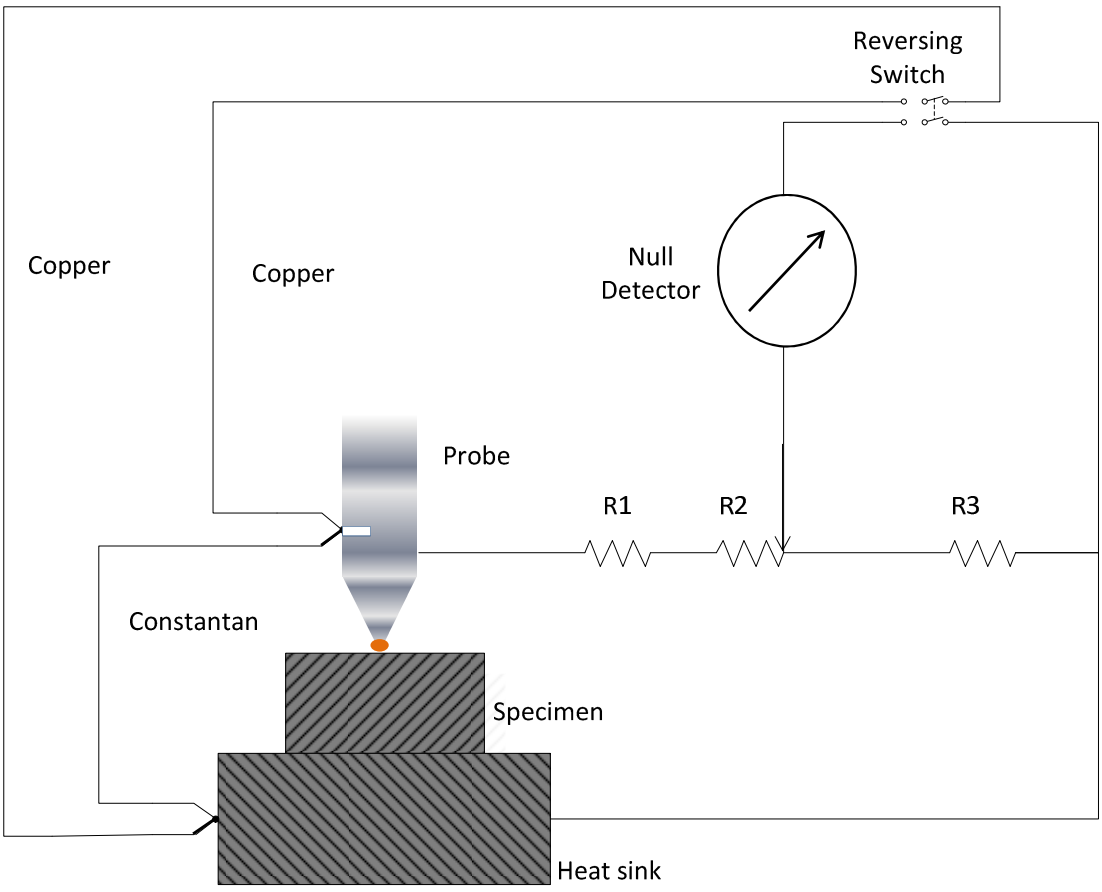

Figure 3.1: Schematic diagram of apparatus for calculating thermopower using a method similar to the Wheatstone bridge circuit [12].

In recent years technological improvements have made it possible for greater resolution (up to 10µm) by similar apparatuses. In their study of functionally graded materials Platzek et.al created the "Seebeck Scanning Microprobe" [13]. The probe is mounted on a three-dimensional micro-positioning system. The system is fully automated; the measurements of the Seebeck coefficient and the position of system are the synchronized by a computer. The probe is heated to create a 3-4 K temperature difference and two copper-constantan thermocouples are used to measure the temperature of the probe (T_1) and temperature of the heat sink (T_0). Two voltages are measured between the Cu-Cu (V_1) connections and the constantan-constantan (V_2) connections. Using these voltages the Seebeck coefficient of the sample was solved in the following manner,

$$S_s = \frac{V_1}{V_2 - V_1}(S_{Cu} - S_{CuNi}) + S_{Cu} \tag{3.1}$$

This apparatus showed a two-dimensional image of the Seebeck coefficient of the surface of the sample. This thesis work focuses on the development of a similar system for characterization of materials and couples fabricated at MSU.

3.3 Room Temperature Thermopower Scanning Probe

3.3.1 Objectives

Using LabVIEW software, the thermopower scanning probe simultaneously measures the voltage across a TE sample and the temperature between a copper probe touching the top surface of the sample and a heat sink beneath the sample. The voltage across the sample will be generated by heating the probe tip to a temperature between 5 – 10^{o}C above the temperature of the heat sink. The thermopower scanning probe uses copper-constantan thermocouples to

measure the temperature of the probe and the heat sink as well as the voltage across the sample. Using these measurements the system determines the thermopower of the sample at specific points such that a thermopower profile for the sample can be measured. The system can be programmed to move vertically and horizontally with respect to the surface of the samples, which allows for greater automation of the measurement.

3.3.2 X-Y-Z Translation Stage and Motors

The thermopower scanning probe is mounted on an X-Y-Z translation stage in order to give it 3-dimensional movement. This allows for scanning in both horizontal and vertical directions with respect to the surface of the samples. The movement is controlled by stepper motors mounted on the stage. The range of motion is 5/8 inches on each axis. The 12 Volt-DC stepper motors are mounted inside the frame of the stage.

Figure 3.2 shows the UCN5804B stepper motor driver used to control the stepper motors. This driver has a simple design which requires only two digital signals; directional control and step input. In this case that digital high-low signal is provided by the National Instruments USB-6501and a LabVIEW program was created to provide a user interface to control the motor using this digital I/O device.

LabVIEW stands for Laboratory Virtual Instrumentation Engineering Workbench and is a software package provided by National Instruments, Inc. This is a graphical programming language that can be used for instrument control, and for data acquisition and analysis. A virtual instrument (VI) is a software routine (or subroutine) that provides an interactive user interface such that software could be programmed to operate similar to the front panel of the instrument it controls. The first step in programming the VI for this stepper motor operation is to calculate the

number of pulses required to move the stage the desired distance. In this case the stepper motor is bipolar, with each step amounting to1.8 degrees, which equals 200 steps per revolution. The stepper motors are attached to the micrometers of an X-Y-Z stage which rotate to move each axis of the stage. One full rotation amounts to one millimeter of travel, which equals 200 steps by the stepper motor. In the VI, the user provides a desired distance and a subroutine calculates how many steps that distance would require. Once the number of steps required is calculated, this value is used as the number of iterations for a loop. Within the loop, two calls to the digital acquisition VI (or subroutine) are fed a high and low command. Figure 3.3 shows a diagram of the digital I/O device and its connection to the stepper motor driver in Figure 3.2. Figure 3.4 shows the layout for a circuit with three drivers which control the automation of the scanning probe. The directional control signal is sent out simultaneously with the step input signal. This works by sending both signals as one package similar to a modulation of signals, where the directional signal acts an envelope for the step inputs carrier signal. There are two directions, each with a high or low value (i.e. left=high, right=low). Once a high or low command is specified, then that direction is sent along with the step input signal.

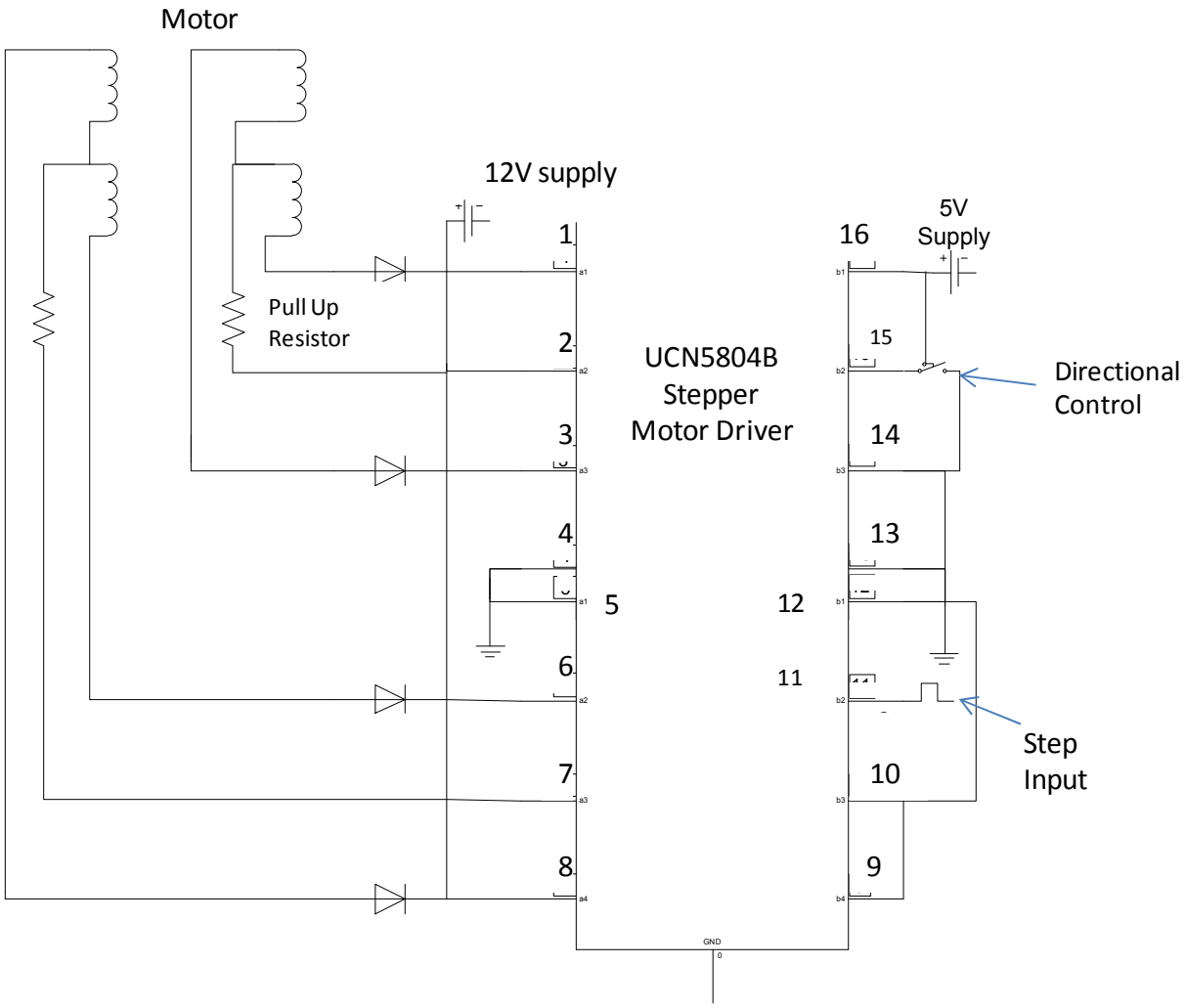

Figure 3.2 UCN5804B Stepper Motor Driver [14]

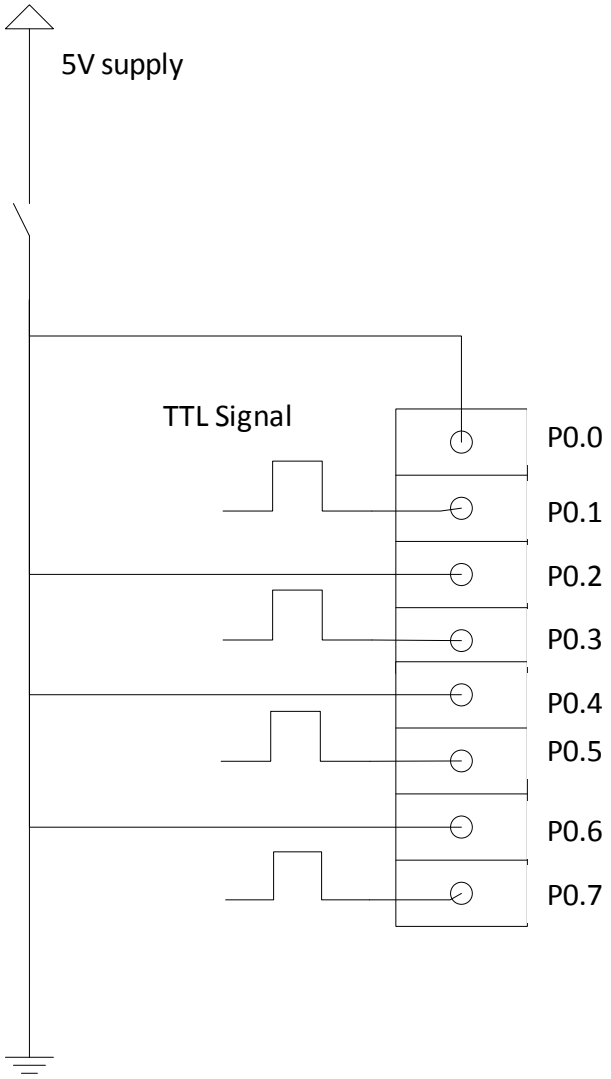

Figure 3.3 National Instruments USB-6501 schematic [15]

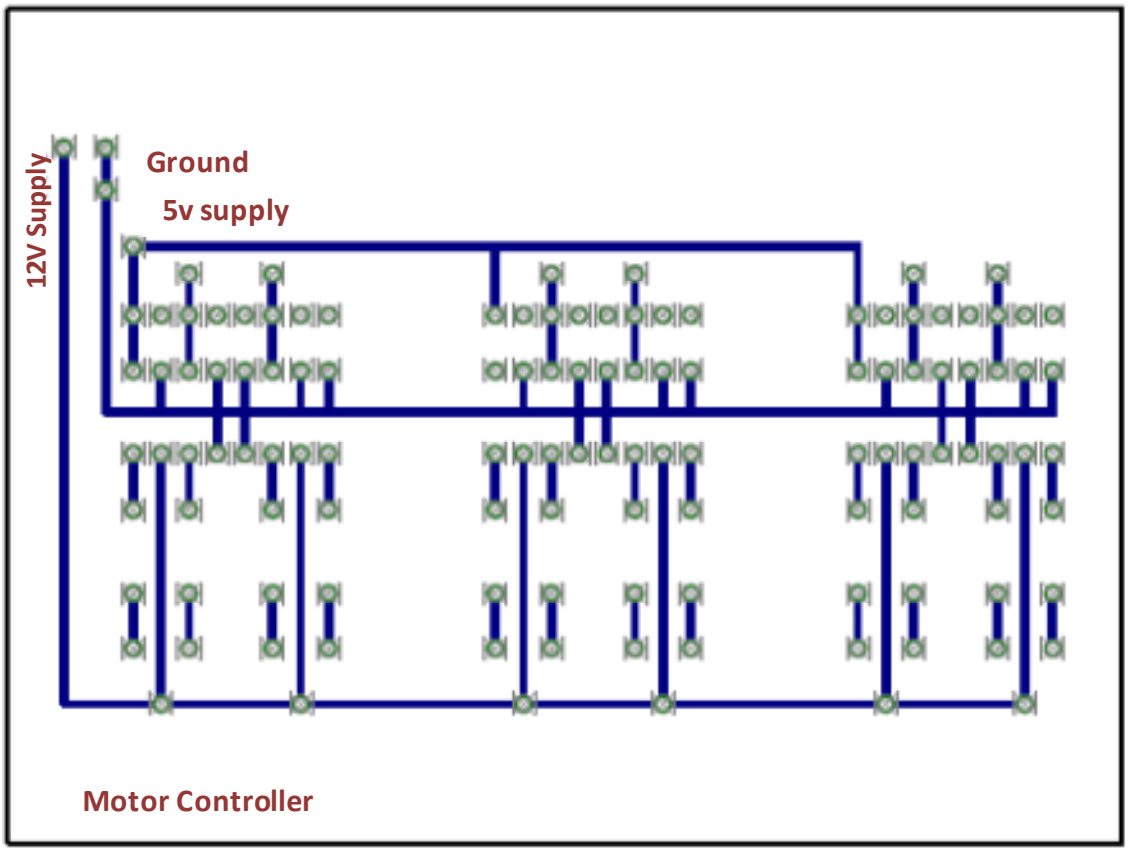

Figure 3.4: X-Y-Z Three Motor Control Printed Circuit Board Layout

3.3.3 Measuring Equipment

Keithley Instruments 2400 Digital Source Meter

This meter has four capabilities: current source, current meter, voltage source and voltage meter. As a source it can supply up to 20 watts of power. For voltage measurements and sourcing it ranges from ±1µV to ±200VDC. For current measurements and sources it ranges from ±10pA to ±1A. It can take readings at a high rate of speed and has on board data storage. It is connected to the computer via a General Purpose Interface Bus (GPIB) connection. In this application the Keithley Instruments 2400 source meter provides current to heat up the probe.

Keithley Instruments 2002 Digital Multimeter

This meter is used only for voltage measurements and provides a resolution ±1µVon the lowest scale setting. This meter contains an optional built in card which allows for ten input channels for measurements, and allows for high speed switching between these channels. The meter has on board data storage for measurement collection and averaging; it is also connected to a computer via GPIB connection. For this system, the 2002 is used to measure thermocouple voltages which range from ±1µV to a few millivolts.

Figure 3.5: Data collection equipment

3.3.4 Probe

A 1” long cone shaped piece of copper with a ¼” diameter is used as the probe. The copper-constantan thermocouple is inserted into the probe through 1mm diameter hole and spark welded to the probe on the sharp end. A nickel chromium wire wound around the probe is used as a heater when current is passed through it, as shown in Figure 3.6. The copper probe and nickel chromium wire are separated by a silicone encapsulate.

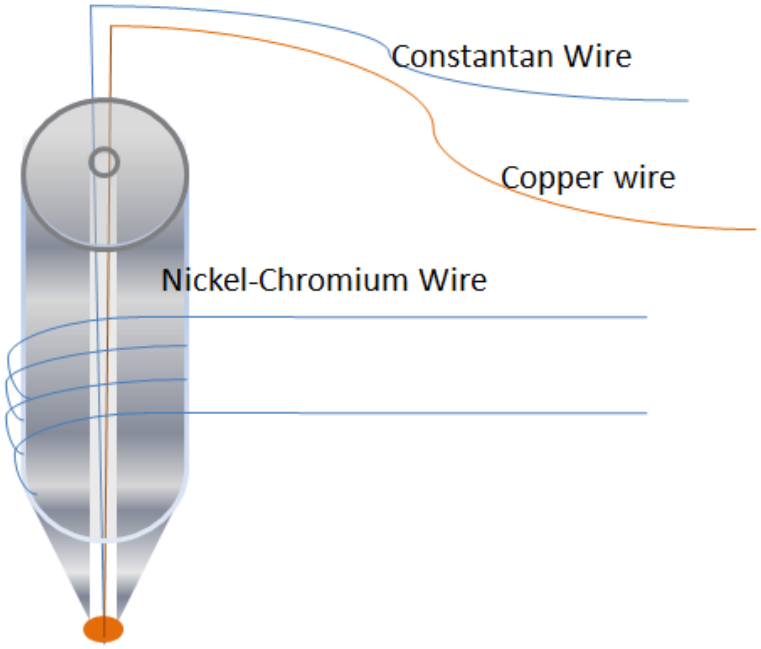

Figure 3.6: Scanning probe design

3.3.5 LabVIEW Program Overview

LabVIEW is a development environment similar to C and BASIC programming languages, but it differs from its counter parts with its graphical language, “G”, where structures of block diagrams and icons are graphically wired together to build the code. This software is commonly used for data acquisition, instrument control, image analysis, data storage, data

analysis, and industrial automation. Subroutines are represented by graphical icons, which are connected by wires for data transmission.

The scanning probe system is fully controlled via PC by LabVIEW. In one program, the movement of the X-Y-Z stage and instrument instruction can be controlled, as well as data collection. Figure 3.7 shows the program flowchart and Figure 3.8 shows the user interface of the LabVIEW program. Some of the more important components of the software can be summarized as follows:

- At room temperature it takes 50-70 seconds for 500 mA of current to heat the probe to a temperature where a satisfactory temperature difference develops between the stage and the probe.
- The system is programmed to begin when the sample is placed on the stage and the probe is touching the top surface of the sample. Beginning the measurements this way takes away the need to measure the distance the probe needs to move up and down to establish a connection with the sample. One way to make sure a connection between the sample and probe is made is to look at the voltage measurements. The voltage readings decline in a steady slope when there is a temperature gradient and conductivity between the probe, sample and stage. If a connection at one of those three points is broken there will be significant noise in the voltage measurements.
- For the motor control, the total distance is the length across the sample in the direction the measurements are taken (i.e. Y-axis). The shift distance is the distance between measurements in the Y direction, the total number of measurements in the Y direction is the total distance divided by the shift distance.

The in/out distance is the distance to move the probe in the X direction to begin a new scan at a different location on the sample. The number of measurements has to be specified so the system can repeat the process for a specified number of locations.

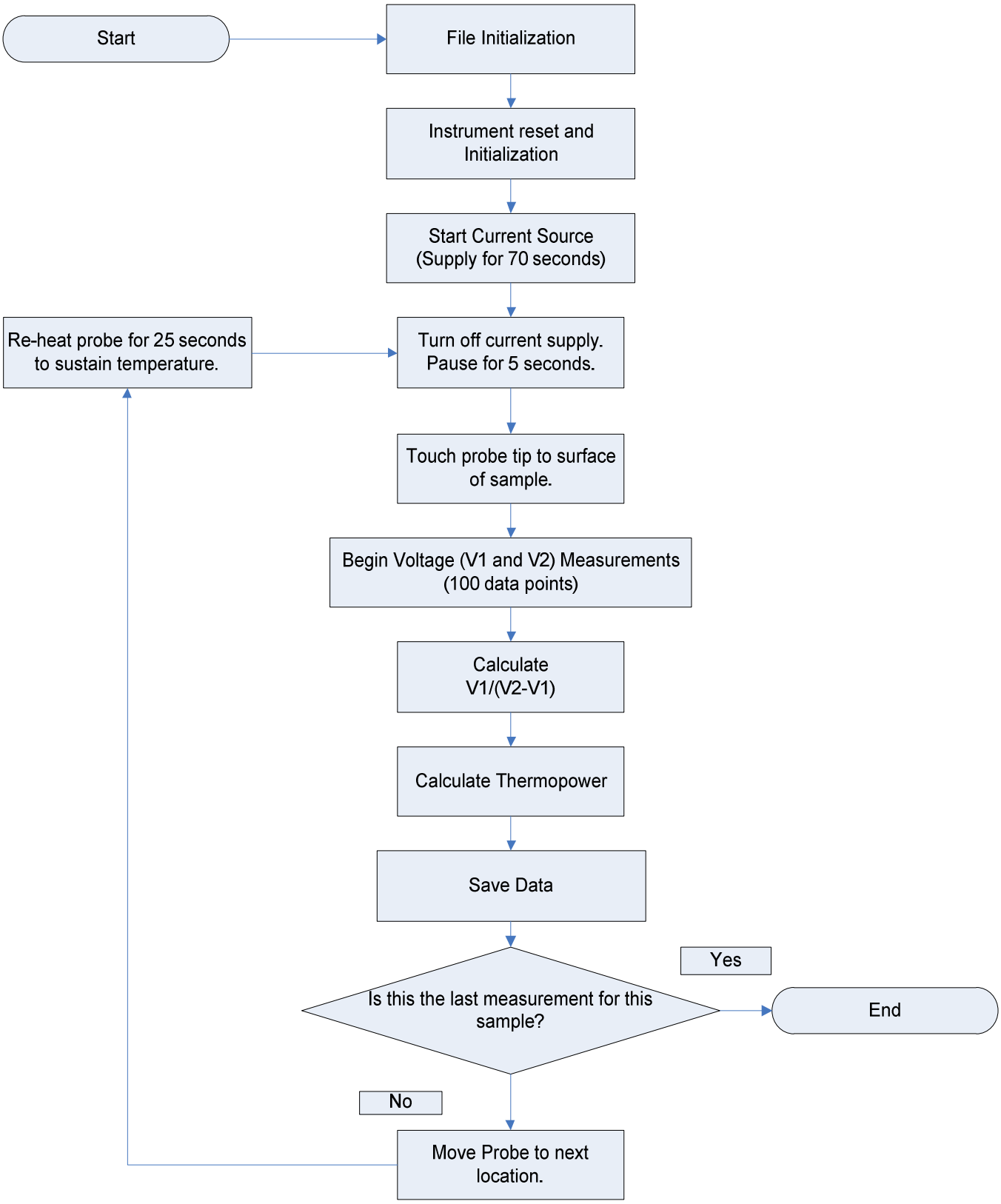

Figure 3.7: LabVIEW software flow chart

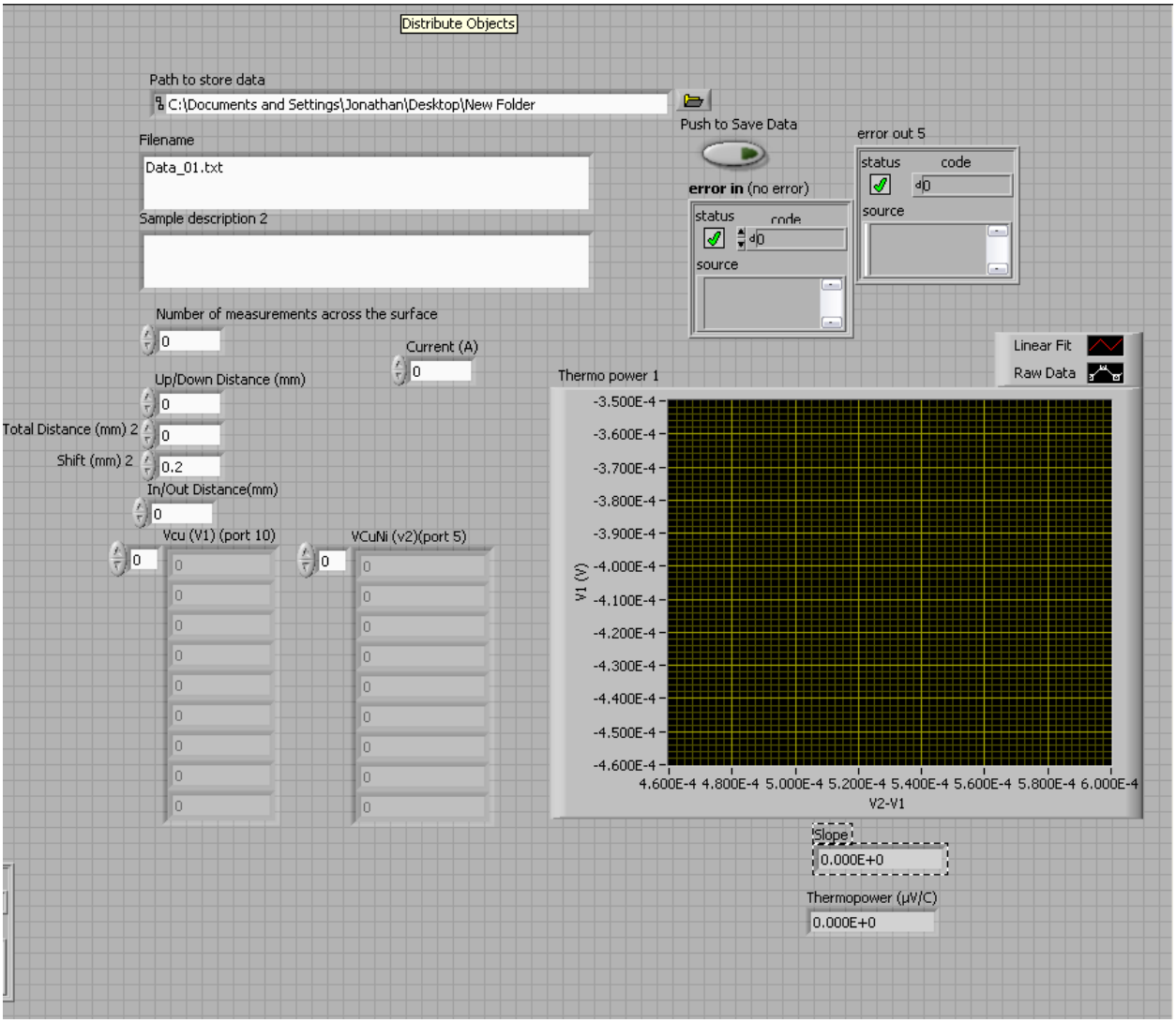

Figure 3.8: LabView user interface.

3.4 Thermopower Calculation Techniques

To determine the thermopower of the sample, measurements of the voltage across the sample and the temperature gradient between hot and cold sides of the sample are taken at a high sampling rate. Temperature measurements can be done directly by measuring thermocouple voltages for the hot and cold sides of the sample and calculating a temperature difference. About 100-300 data points are taken for each measurement point and a fit of this data is made. Figure

3.9 and 3.10 show this graphically, where Figure 3.9 is the data taken and Figure 3.10 is the linear fit of the data.

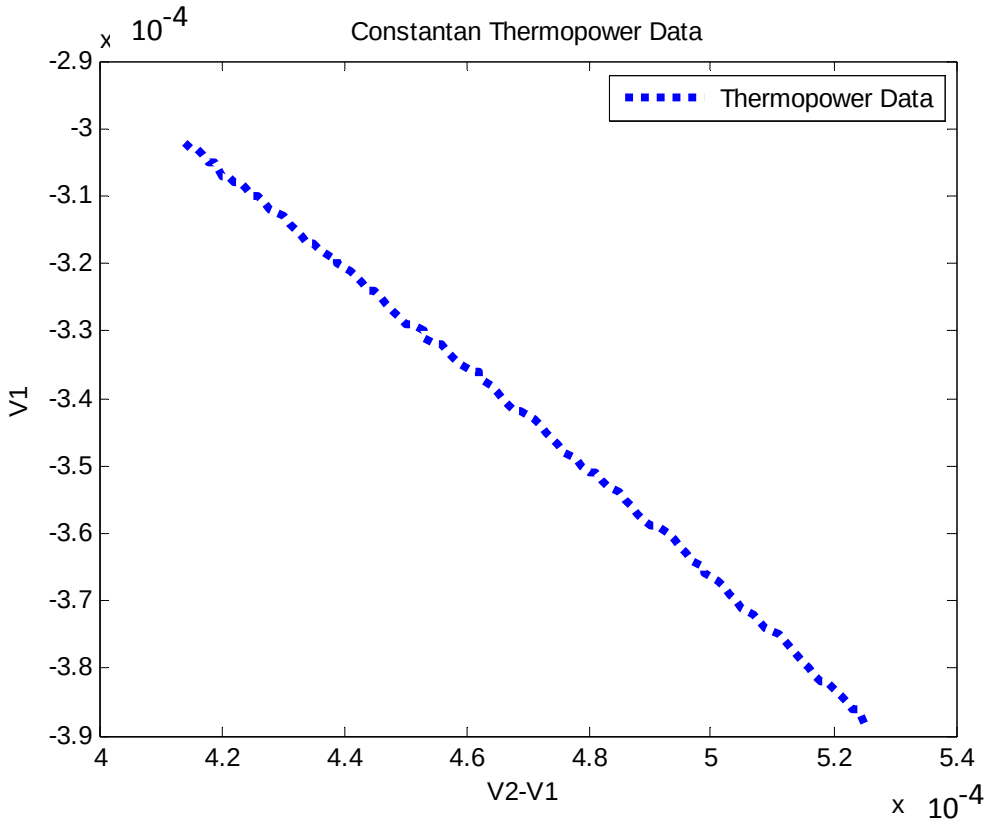

Figure 3.9: Scatter plot of V1/(V2-V1) data.

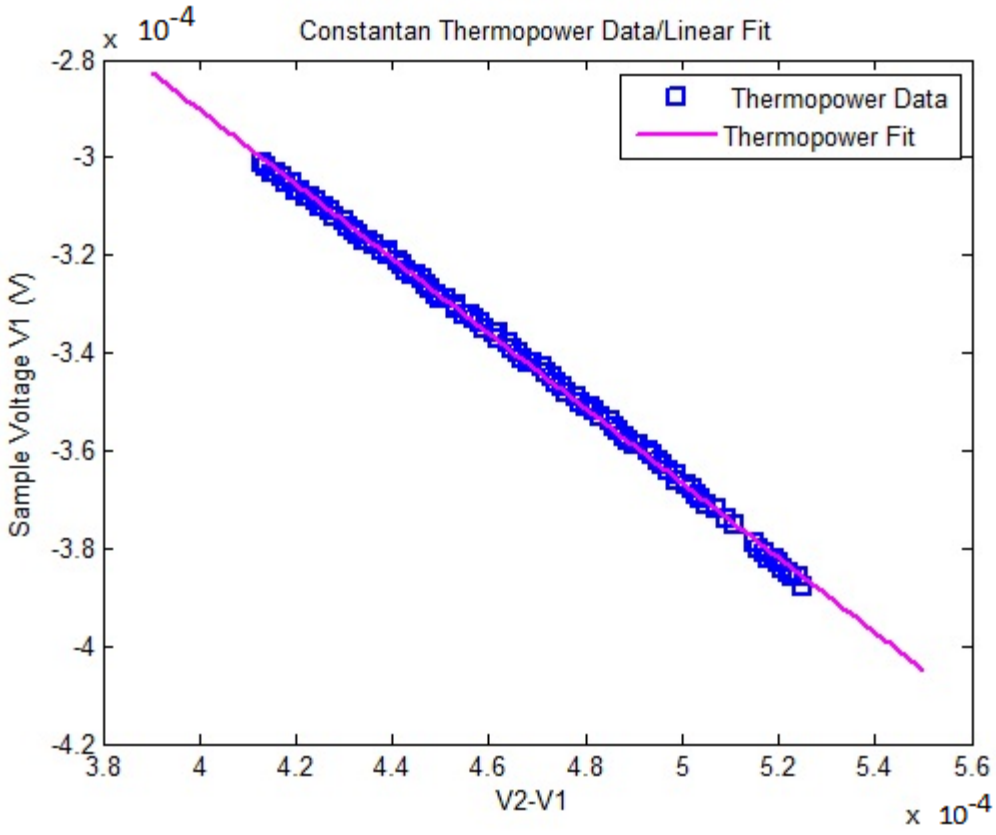

Figure 3.10: Scatter plot of V1/(V2-V1) data with linear fit.

3.4.1 Pulsed technique for measuring thermopower [16]

One method used to measure thermopower is a pulsed technique where two thermocouples are used to measure the thermopower in a homogeneous bulk material [16]. The mounting configuration is shown in Figure 3.11 for type-T thermocouples.

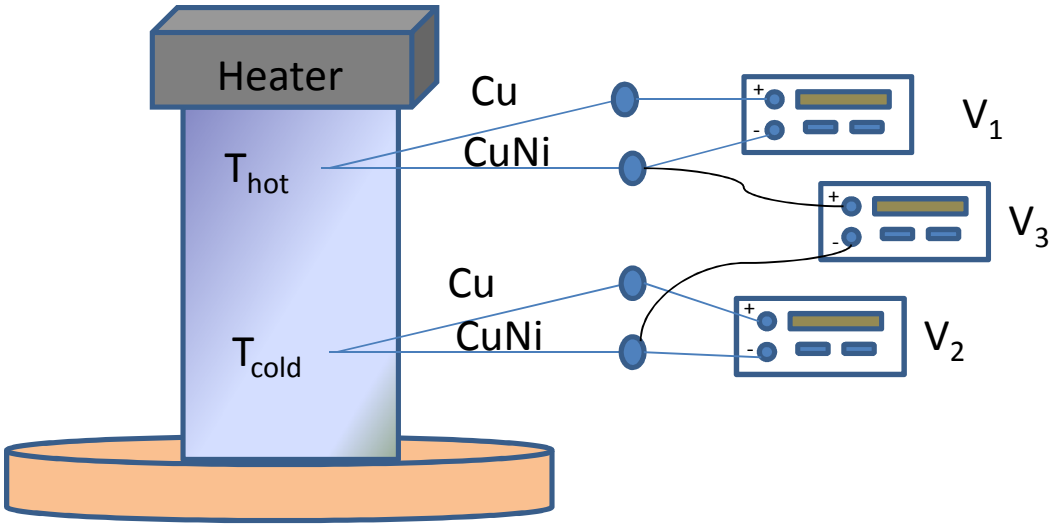

Figure 3.11: Pulsed technique measurement diagram.

In the above figure three voltage measurements are taken with two thermocouples. The thermocouples are copper (Cu) -constantan (CuNi). An RTD provides the heat for the hot side of the sample. The thermopower is measured by supplying pulsed heat across the sample (the RTD is turned on and of periodically). Over time the difference in temperature across the sample will maintain a stable periodic function with a constant offset. This method allows for a 1K difference between the hot side and cold side temperature, this temperature gradient and the voltage across the sample are used to calculate the thermopower of the sample. The advantage behind measuring thermopower with this technique is it eliminates any unknown temperature gradients along the measuring wires by using the slope of many data points in the calculation of thermopower, and ignoring the y-axis offset. This method also eliminates any D.C. offsets that might exist in the measurement meters. The calculation of thermopower using this method can be shown mathematically as:

$$V_1 = \int_{T_R}^{T_H} S_{Cu}(T)dT + \int_{T_H}^{T_R} S_{CuNi}(T)dT = \int_{T_R}^{T_H} [S_{Cu}(T)dT - S_{CuNi}(T)]dT \qquad (3.6)$$

$$V_2 = \int_{T_R}^{T_C} S_{Cu}(T)dT + \int_{T_C}^{T_R} S_{CuNi}(T)dT = \int_{T_R}^{T_C} [S_{Cu}(T)dT - S_{CuNi}(T)]dT \quad (3.7)$$

$$V_1 - V_2 = \int_{T_R}^{T_H} [S_{Cu}(T)dT - S_{CuNi}(T)]dT - \int_{T_R}^{T_C} [S_{Cu}(T)dT - S_{CuNi}(T)]dT \quad (3.8)$$

$$= \int_0^{T_H} S_{TC}(T)dT - \int_0^{T_R} S_{TC}(T)dT - \int_0^{T_C} S_{TC}(T)dT - \int_0^{T_R} S_{TC}(T)dT = \int_{T_C}^{T_H} S_{TC}(T)dT$$

$$\int_{T_C}^{T_H} S_{TC}(T)dT \approx S_{TC}(T_{AVG}) \cdot (T_H - T_C), (T_{AVG}\text{= average temperature}) \quad (3.9)$$

$$T_H - T_C \ll T_{AVG} \equiv \frac{T_1 + T_2}{2}$$

$$\rightarrow S_{Sample}(T_H) \approx S_{Sample}(T_C) \text{ and } S_{CuNi}(T_H) \approx S_{CuNi}(T_c) \quad (3.10)$$

$S_{Sample}(T)$ *and* $S_{CuNi}(T_H)$ are constant over ΔT.

$$V_1 - V_2 = S_{TC}(T_H - T_C) = S_{TC}(T_{AVG}) \cdot \Delta T \quad (3.11)$$

The difference between V_1 and V_2 in this technique equals the thermopower of the thermocouples used multiplied by the temperature gradient between the two thermocouples. In the technique V_1 and V_2 provide the temperature gradient needed to calculate thermopower of the sample, to solve for the voltage difference you need a third voltage measurement V_3, which is derived as follows:

$$V_3 = \int_{T_R}^{T_H} S_{CuNi}(T)dT + \int_{T_H}^{T_C} S_{Sample}(T)dT + \int_{T_C}^{T_R} S_{CuNi}(T)dT \quad (3.12)$$

$$= \int_0^{T_H} S_{CuNi}(T)dT - \int_0^{T_R} S_{CuNi}(T)dT - \int_{T_C}^{T_H} S_{Sample}(T)dT + \int_0^{T_R} S_{CuNi}(T)dT - \int_0^{T_C} S_{CuNi}(T)dT$$

$$= -\int_{T_C}^{T_H} S_{Sample}(T)dT + \int_{T_C}^{T_H} S_{CuNi}(T)dT$$

when $T_H - T_C \ll T_{AVG} \equiv \frac{T_1+T_2}{2} \rightarrow S_{TC}(T_H) \approx S_{TC}(T_C)$, $S_{TC}(T_H)$ is a constant. Assuming the sample thermopower and platinum thermopower are constant over a small temperature gradient then

$$V_3 = [S_{CuNi}(T_{AVG}) - S_{Sample}(T_{AVG})] \cdot \Delta T \tag{3.13}$$

Finally to solve for the thermopower of a sample, (3.8) is used in (3.13) to give,

$$S_{Sample}(T_{AVG}) = S_{CuNi}(T_{AVG}) - \frac{V_3}{\Delta T} = S_{CuNi}(T_{AVG}) - \frac{V_3}{\left(\frac{V_1 - V_2}{S_{TC}(T_{AVG})}\right)}$$

$$= S_{CuNi}(T_{AVG}) - \frac{V_3}{V_1 - V_2} \cdot S_{TC}(T_{AVG}) \tag{3.14}$$

V_3 and (V_1-V_2) are non-linear functions by themselves but they have a linear relation to each other. When $T_H - T_C \ll T_{AVG} \equiv \frac{T_1+T_2}{2} \rightarrow S_{Sample}(T)$is constant, thus the slope $\frac{\Delta V}{\Delta T}$ is constant. In this technique V_3 and (V_1-V_2) are plotted against each other which results in a linear function. The thermopower is calculated by taking 200-300 data points for V_3 and (V_1-V_2), taking the best fit of the linear function and finding the slope of that linear function.

As stated before the advantage of this method, is it eliminates spurious voltages caused by unknown temperature gradients along the measuring wires. This method is used in various measurements systems and provides accurate thermopower measurements from room temperature to very high temperatures. The disadvantage to this method is it requires the sample being measured to have homogeneous composition in order to have accurate measurements. This can be problematic when samples are inhomogeneous, i.e. samples made of segmented material. The following sections will present methods for measuring thermopower, which allow for measurements of homogeneous and inhomogeneous bulk TE material.

3.4.2 Method of Measuring Thermopower Using Direct ΔT Measurements

In this technique direct voltage measurements are taken by a probe and separate temperature measurements are taken for the temperature gradient. Since only one meter is used to take both measurements, the meter needs to be able to switch between two measurements very quickly. This method does not provide instantaneously corresponding voltage and temperature measurements as the pulsed technique, but the high speed switching between the two measurement ports provides reasonable measurements that are comparable to those found using multiple meters to collect instantaneous voltage and temperature gradient data.

The two voltages taken are the voltage across the sample and the voltage of the copper-constantan thermocouple. Using the procedure outlined in section 2.8.4, the thermocouple voltage is converted to the hot side temperature. The cold side temperature is measured by a resistance temperature detector (RTD), which is attached to the heat sink. The difference between the hot and cold side temperatures is the value of ΔT. For this technique, the slope of the data is what determines the value of the thermopower. Taking over 100 ΔV/ΔT data points, a thermopower measurement for a single point is made where the probe tip touches the surface of

the samples. Over time the heat from the probe permeates the sample from the point of contact between the probe and the sample. Taking many measurements from a single point of contact shows the gradual decline in temperature and voltage as the sample absorbs the heat from the probe. A linear fit to the ΔV vs. ΔT data then gives a slope that is a Seebeck voltage of the copper to sample junction. The thermopower of the sample is then determined by removing the contribution from the copper leads.

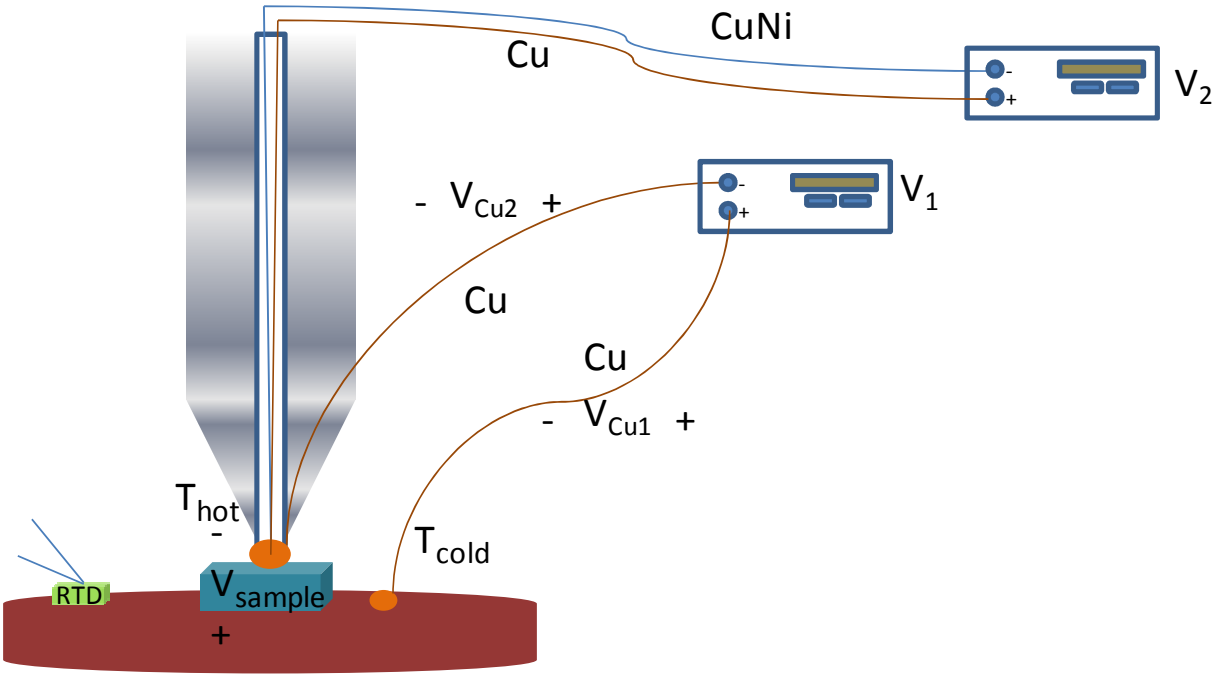

Figure 3.12: An illustration of the Method of Measuring Thermopower Using Direct ΔT Measurements

One disadvantage to this method is the inability to properly analyze high inaccuracies for lower thermopower samples. This can be explained by breaking down the voltage measurement of the sample; illustrated in Figure 3.12. Using Kirchhoff's voltage law the expression for the voltages in the loop is as follows:

$$V_{measured} - V_{Cu1} - V_{sample} + V_{Cu2} = 0 \qquad (3.15)$$

The voltages in equation (3.15) can be written in terms of the thermopower and temperature using equation (2.2). This leads to an expression for the voltage measured by the volt meter.

$$V_{measured} = \int_{T_o}^{T_c} S_{Cu1}dt + \int_{T_c}^{T_H} S_{sample}dt + \int_{T_H}^{T_o} S_{Cu2}dt$$

$$= \int_{T_C}^{T_H} S_{sample}dt + \int_{T_H}^{T_C} S_{Cu}dt \quad (3.16)$$

The voltage due to the copper wires can be written as:

$$-\int_{T_C}^{T_H} S_{Cu}dt$$

This leads to the following equation for the voltage measured by the meter.

$$V_{measured} = S_{sample}(\Delta T) - S_{Cu}(\Delta T) \quad (3.17)$$

The true voltage across the sample is given by the following expression.

$$S_{sample}(\Delta T) = V_{measured} + S_{Cu}(\Delta T) \quad (3.18)$$

This voltage takes into account the added contribution of the Cu leads*.

The measurements in Figure 3.13 show the value of $V_{measured}$ for a reference sample of constantan (-39.5μV/K at 300K). The measurements range from -31μV/K to -33μV/K and Figure 3.14 show the measured thermopower values for constantan after correction for the copper leads. These thermopower values range from -28μV/K to -31μV/K, which differ from the reference value by 20%-26% respectively. It is important to note that these errors are less pronounced when the samples thermopower is higher that ±100μV/K. These large errors can

*The thermopower of Cu is 1.97μV at room temperature.

lead to unreliable measurements for samples with smaller thermopower. Also it can be very time consuming and inefficient to calculate how much the addition of the copper connection wires thermopower affects the overall data.

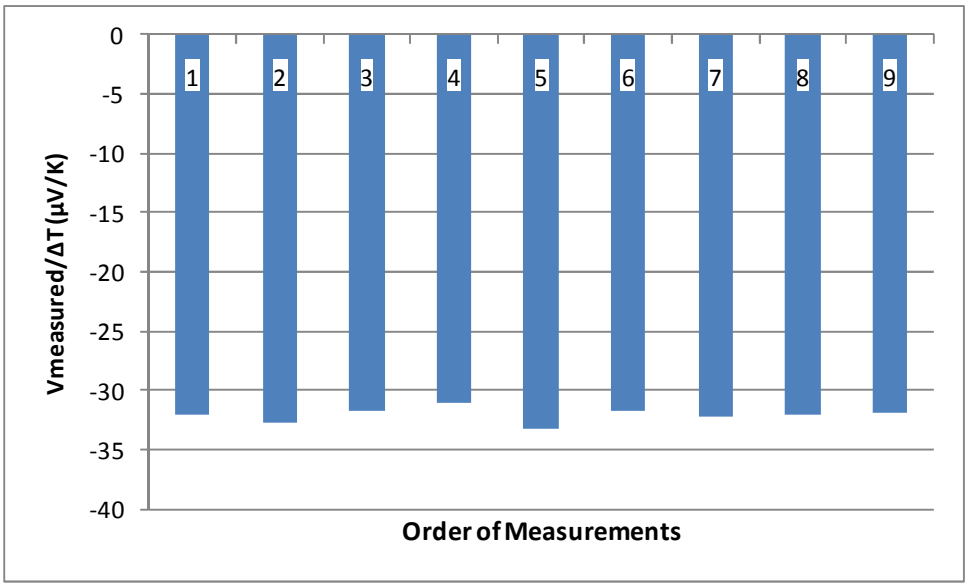

Figure 3.13: Voltage/ΔT data of constantan sample with the Cu contribution not yet removed.

Figure 3.14: Corrected constantan thermopower data.

While using this method finding the cause of measurement errors was very difficult. The issue did not become apparent until a different method was attempted. This method will be introduced in the following section and measurement results will be presented in chapter 4.

3.4.3 Thermocouple Method for Measuring Thermopower

To investigate improvements to the accuracy of the system the RTD used to measure the base temperature was replaced with a copper-constantan thermocouple. Similar to the method presented in [13], two copper-constantan thermocouples were used to measure the hot and cold side temperatures. Using equations the following equations

$$V_1 = (S_s - S_{Cu}) \cdot (T_1 - T_0) \tag{3.2}$$

$$V_2 = (S_s - S_{CuNi}) \cdot (T_1 - T_0) \tag{3.3}$$

$$\frac{(S_s - S_{Cu}) \cdot (T_1 - T_0)}{(S_s - S_{CuNi}) \cdot (T_1 - T_0) - (S_s - S_{Cu}) \cdot (T_1 - T_0)} = \frac{V_1}{V_2 - V_1}$$

$$S_s = \frac{V_1}{V_2 - V_1}(S_{Cu} - S_{CuNi}) + S_{Cu}$$

The thermopower of the sample can be solved directly using the slope of $V_1/(V_2 - V_1)$ as shown in Figure 3.15, and the thermopower of constantan and copper. This also helps eliminate errors that can be created by erroneous temperature measurements. The measurement results using this method will be presented in chapters four and five.

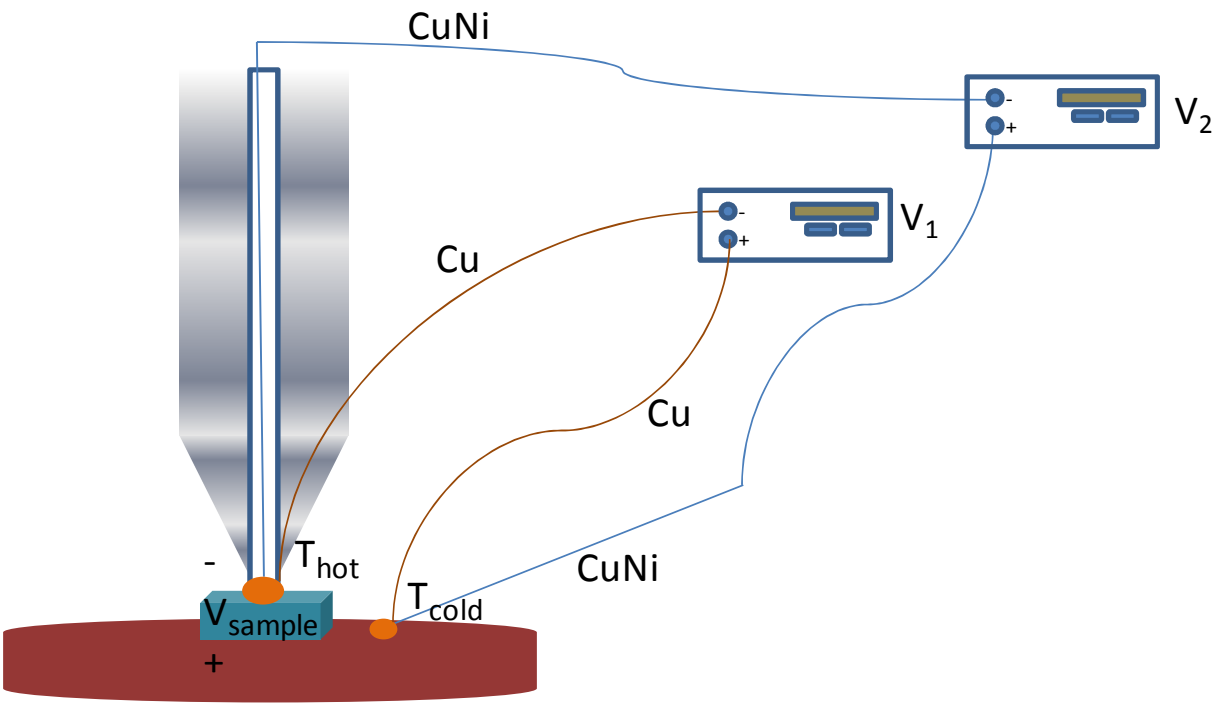

Figure 3.15: An illustration of the Thermocouple Voltage Measurements Method for Calculating Thermopower using copper-constantan thermocouples.

Chapter 4: Reference measurements

4.1 Introduction

To test that the system is operating as desired, thermopower values of various metals and alloys were used as references. The ideal material for reference measurements are high purity metals or alloys with thermopower values that remain constant over time regardless of the method of which the material was formed. For example the thermopower values of Cu, Pb and Pt have been known for decades, if measurements of a high purity sample made of one these metals is taken with various systems in labs across the country, a result matching published data would be considered reliable since these materials have been used as standard reference materials in research. Another good candidate for reference measurements is the alloy constantan, which will be explored further in a later section. Using well known thermoelectric materials (i.e. Si-Ge, PbTe) as reference material is an unreliable method of checking the accuracy of a system since there can be significant variation in the properties of the samples even when made by the same process. There are no standard reference materials for high thermopower materials even though Bi_2Te_3 has recently come into consideration to be named as a standard reference material [17]. The following criterion for acceptable standard reference materials was developed by NIST [18]:

- First it was determined that the material should be able to achieve long term stability and be homogenous, for reproduction at a large scale.
- The standard reference material should be able to have a thermopower value regularly measured in the field (between 25μV/K and 400μV/K).
- A thermoelectric standard reference material should be reasonably available to the research community as far as cost is concerned.

- Lastly a standard reference material has to be able to be used in the future for development of reference materials for broader and different temperature ranges.

Most thermoelectric materials are tailor made with specific optimizations in mind, i.e. doping concentration, annealing time, etc. Even though thermoelectric materials might not be useful as reference samples for absolute thermopower measurements, they can be useful in measuring the polarity of a material due to their high thermopower values. The polarity of the voltage measurement of a sample is the indicator that shows if the sample is n-type or p-type.

4.2 Bi_2Te_3 Reference Measurements

Bi_2Te_3 samples from the Tellurex Corporation were used to check if the system would produce a voltage measurement with the proper polarity. Samples with dimensions of 5mm × 5mm × 2mm were used to check for n-type and p-type polarity. For the n-type measurement, a single point on the surface of the sample was measured. The resulting slope of $V_1/(V_2-V_1)$ was negative indicating that the sample was indeed n-type, and the magnitude was reasonable for these samples as shown in Figure 4.1.

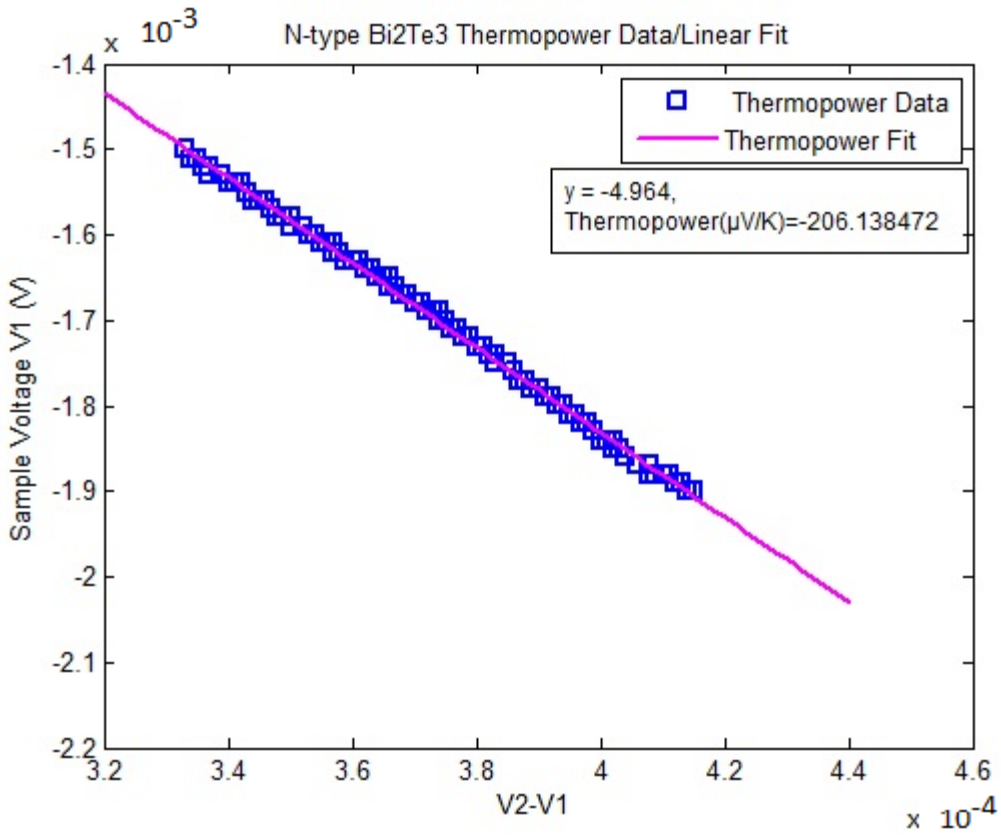

Figure 4.1: N-type Bi_2Te_3 reference measurement.

Likewise for the p-type sample, the resulting slope of $V_1/(V_2-V_1)$ was positive indicating that the sample was p-type and the value of the thermopower was 220μV/K which is in good agreement with high quality p-type Bi_2Te_3 materials.

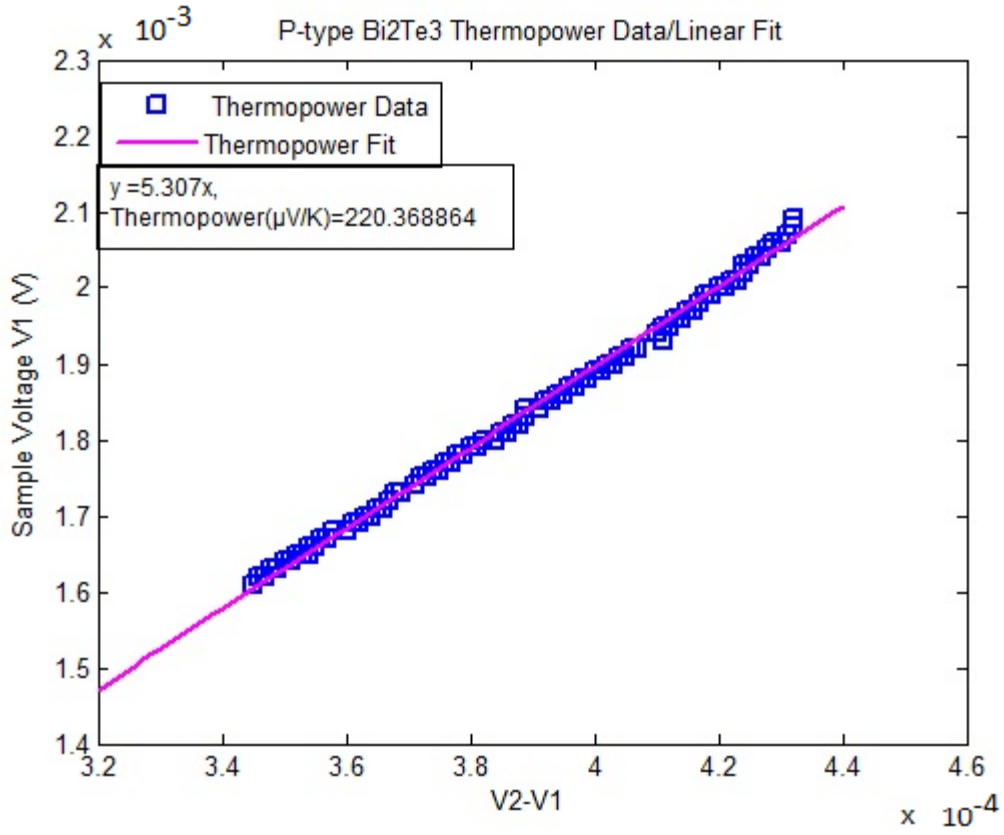

Figure 4.2: P-type Bi_2Te_3 reference measurement.

4.3 Constantan

Constantan is an alloy composed of 55% Cu and 45% Ni, it is a suitable material for reference measurements in this system because it is commonly fabricated, reproducible, and is stable in time. Constantan is an n-type material, with a thermopower of -39.5μV/K at room temperature. A fit for the thermopower of constantan was determined for a wide temperature range using the thermopower of a type T thermocouple and Cu [16]. The thermopower of a type T thermocouple is the difference between the thermopower of Cu and constantan. The thermopower of Cu was published by Roberts [19]; the literature also provided a thermopower scale for temperatures ranging from room temperature to 900K. The thermopower of thermocouples can be calculated by using data provided by NIST for thermocouple voltages

versus temperature for a wide range of thermocouple types. Table 4.1 shows the ninth order polynomial coefficients for the fit of the thermopower of constantan over a wide temperature range and Figure 4.3 shows the thermopower data from 290K to 680K.

Table 4.1: The coefficients for the fit of the thermopower of constantan [16]

Y = M0+M1*x+….+M8*x^{8}+M9*x^{9}	
M0	-996.557
M1	13.94639
M2	-0.08016
M3	0.000223
M4	-2.45E-07
M5	-2.18E-10
M6	9.67E-13
M7	-1.12E-15
M8	5.38E-19
M9	-7.47E-23
R	0.999999984

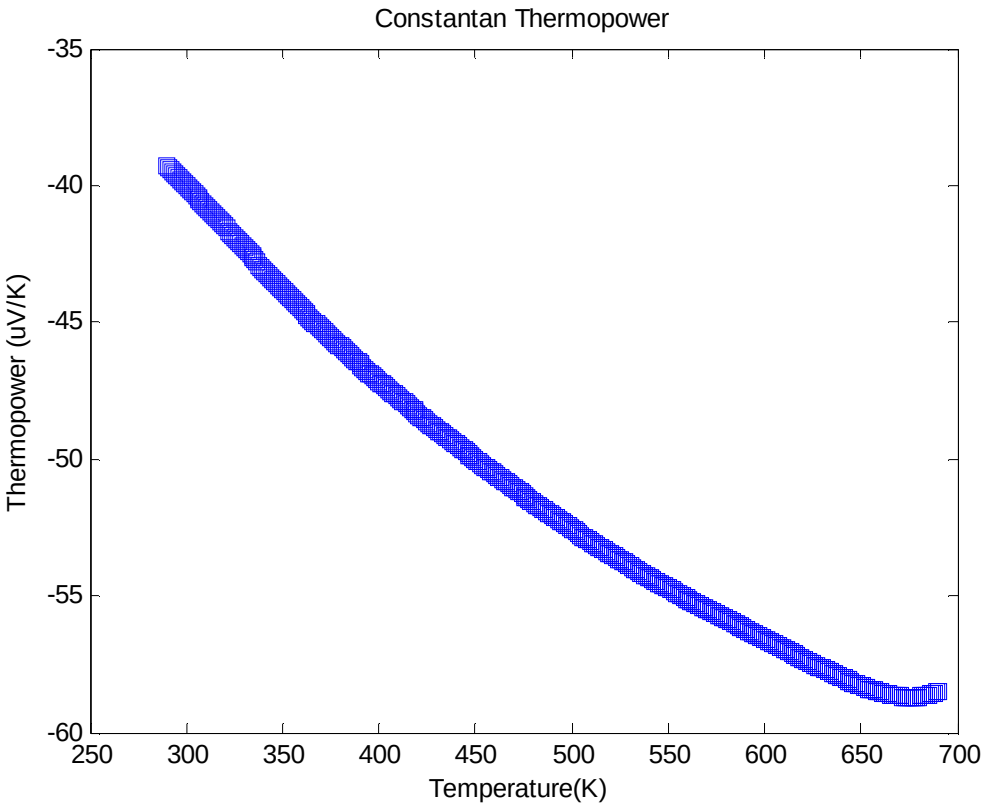

Figure 4.3: The thermopower of constantan from 290K to 680K.

An 8.1mm diameter × 3.1mm thick cylindrical piece of 99.999% pure constantan was used as a reference sample (see Figure 4.4).

Figure 4.4: cylindrical piece of constantan.

Figure 4.5 shows ten measurements of constantan using the thermopower scanning probe.

Figure 4.5: Constantan thermopower data.

The measurements range from -31μV/K to -33μV/K, with the average being -32.458μV/K This corresponds to an error between 20%-15% from the reference -39.5μV/K, with the average error of the ten measurements being 17.94%.

Figure 4.6: Constantan measurement errors.

Using the method presented in section 3.4.4 the thermopower of constantan fell reliably within the range presented in Figure 4.5. These measurements for constantan are important because they help to show the limits of accuracy of this system.

4.4 Low thermopower material measurements

Metals such as Cu and Pb were measured and the error between measured thermopower values and expected values was substantially larger than the error found for the constantan measurements. Cu has a room temperature thermopower value of 1.97μV/K and Pb has a room temperature thermopower of -1.05μV/K [19]. When the thermopower of these two metals were measured using the thermopower scanning probe, a measurable thermopower could not be detected. Lower thermopower values of a sample correlated to higher the measurement error while using this method to measure thermopower.

4.5 Error Analysis

To begin to understand the errors in these measurements, the key components of this measurement technique have to be explained in detail. As stated in the previous chapter the two voltages are defined as

$$V_1 - V_{Cu1} - V_{sample} + V_{Cu2} = 0 \text{ and}$$

$$V_2 - V_{CuNi1} - V_{sample} + V_{CuNi2} = 0$$

As shown in section 3.4.3, these equations can be represented the following way

$$V_1 = S_s \cdot (\Delta T) - S_{Cu} \cdot (\Delta T)$$

$$V_2 = S_s \cdot (\Delta T) - S_{CuNi} \cdot (\Delta T)$$

This results to the following representation which will be used for the remainder of this thesis:

$$V_1 = (S_s - S_{Cu}) \cdot (T_1 - T_0)$$

$$V_2 = (S_s - S_{CuNi}) \cdot (T_1 - T_0)$$

From the above equation the temperature gradient is calculated in the following manner

$$V_2 - V_1 = (S_s - S_{CuNi}) \cdot (T_1 - T_0) - (S_s - S_{Cu}) \cdot (T_1 - T_0)$$

$$\Delta T = \frac{V_2 - V_1}{(S_{Cu} - S_{CuNi})} \tag{4.1}$$

Using the above equation for the temperature gradient, the expected values of ΔT can be calculated for $V_2 - V_1$ values (as shown in Figure 4.7).

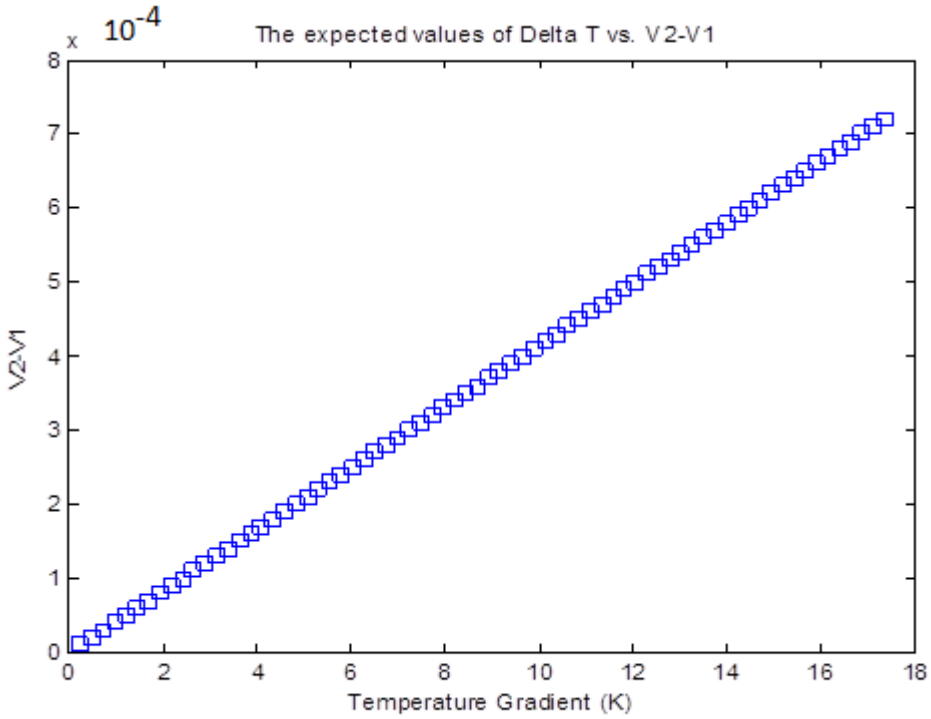

Figure 4.7: The expected values of ΔT vs. $V_2 - V_1$.

While doing reference measurements, the samples with the largest percent errors from the expected values were those with low thermopower values. The source of this error can be explained using the thermopower of copper and constantan and the above equations for V_2 and V_1.To begin, the expected values of copper can be calculated in the following manner.

$$V_1 = (1.97\mu V/K - S_{Cu}) \cdot (T_1 - T_0)$$

$$V_2 = (1.97\mu V/K - S_{CuNi}) \cdot (T_1 - T_0)$$

For the range of ΔT values shown in Figure 4.7, the corresponding values of V_2 and V_1 are shown in Figure 4.8.

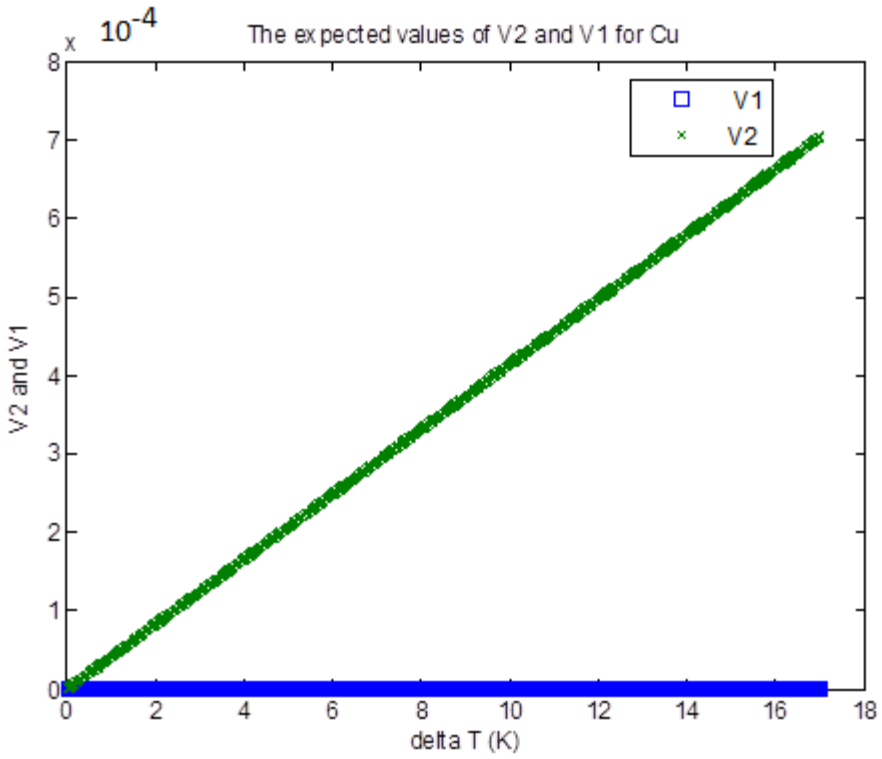

Figure 4.8: Expected values of V_1 and V_2 for Cu

When a copper sample was measured using the thermopower scanning probe the measured value had a very high error with respect to its expected value. Looking closer at the data, the voltage values for V_1 and V_2 were offset in a negative direction with respect to their expected values. This offset was equal in magnitude for both V_1 and V_2 as shown in Figure 4.9.

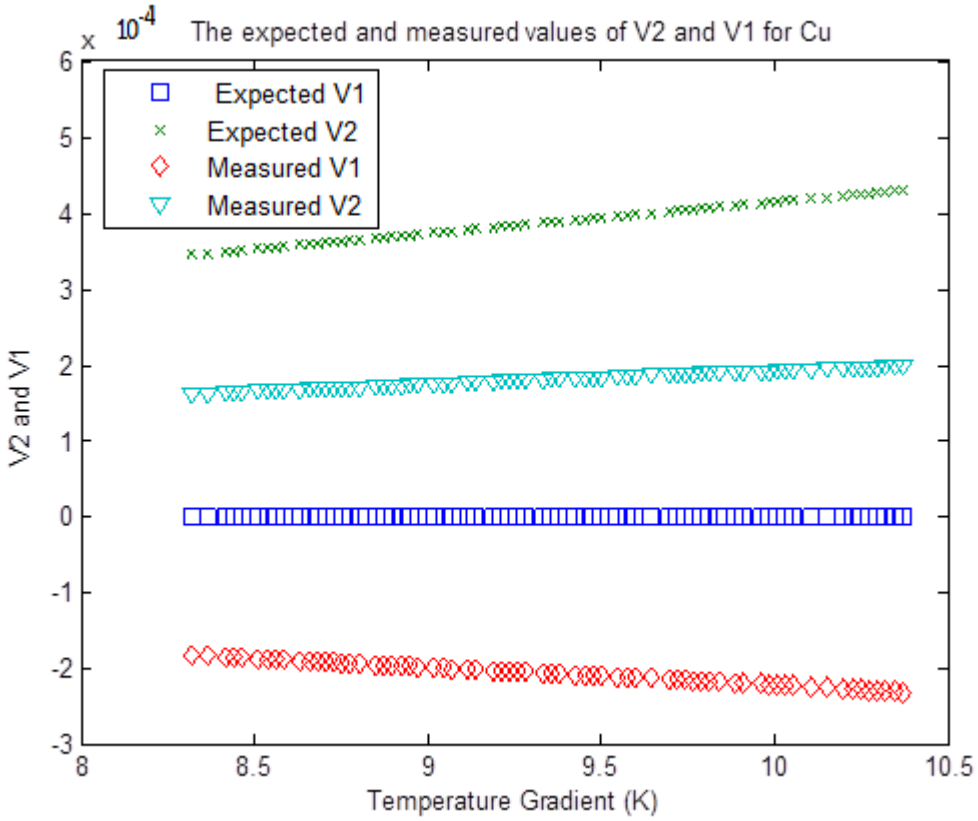

Figure 4.9: Expected and measured values of V_1 and V_2 for Cu.

The expected value of V_1 value is zero but for all measurements the values of V_1 and V_2 are offset from 200µV to 160µV in the negative direction with respect to their expected values. Although it might seem that the offset is decreasing, this does not mean that the error can be reduced with a decreasing temperature gradient since the calculation of the temperature gradient

depends on $V_2 - V_1$. Figure 4.9 shows a snapshot of the voltage measurements at a ΔT between 8 and 10K. Using the same procedure used to calculate the expected value of copper, the expected values of V_1 and V_2 for constantan are shown in Figure 4.10.

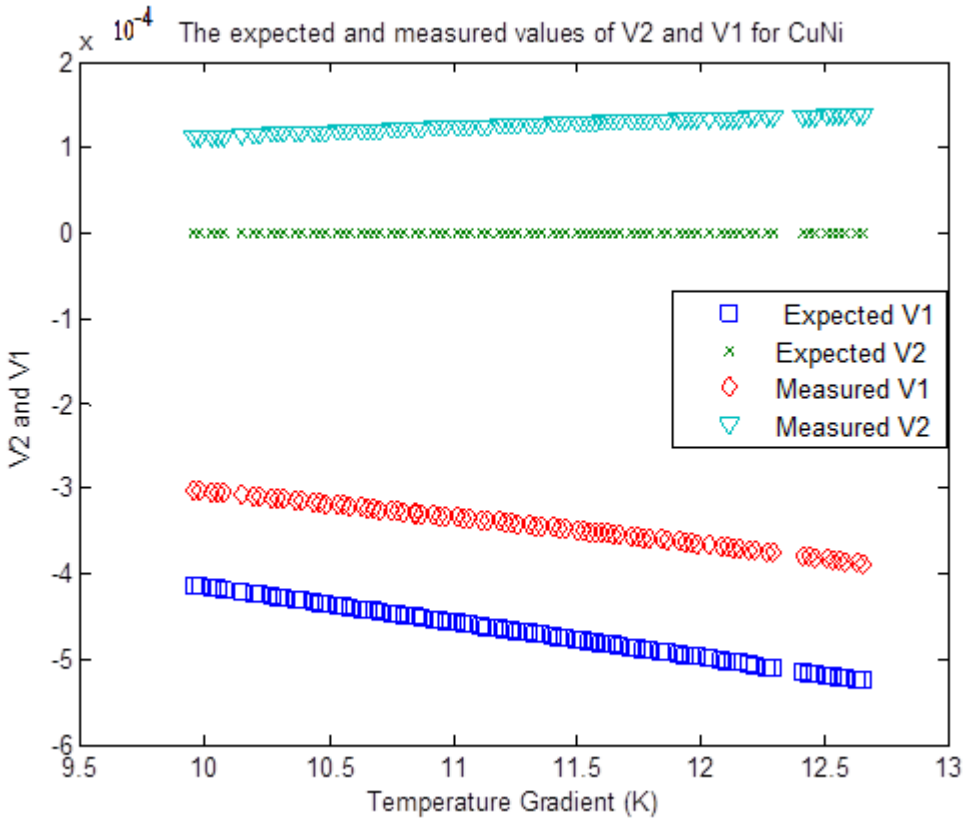

Figure 4.10: Expected and measured values of V_1 and V_2 for constantan.

The offset for constantan was shifted to more positive voltages than expected (Figure 4.10), while the offset for the copper sample was to more negative voltages than expected (Figure 4.9). In Figure 4.11 it can be seen that the magnitude of the offset correlates with the increase in voltage magnitude; as the temperature gradient increases the magnitudes of the measured voltages for V_1 and V_2 increase. Figure 4.11 shows the 100 V_1 and V_2 measurements used to

calculate each thermopower values in Figure 4.5. This data shows the effect of the temperature gradient to the voltage magnitude. The initial measurements were done while the probe was cool, which led to a smaller temperature gradient. The probe was heated with a specific amount of current for a short amount of time, lowered to the surface of the sample and these measurements were taken. Some measurements were taken consecutively, repeating the same process after a short break which caused the probe temperature to rise; as a result some measurements had higher temperature gradients than others.

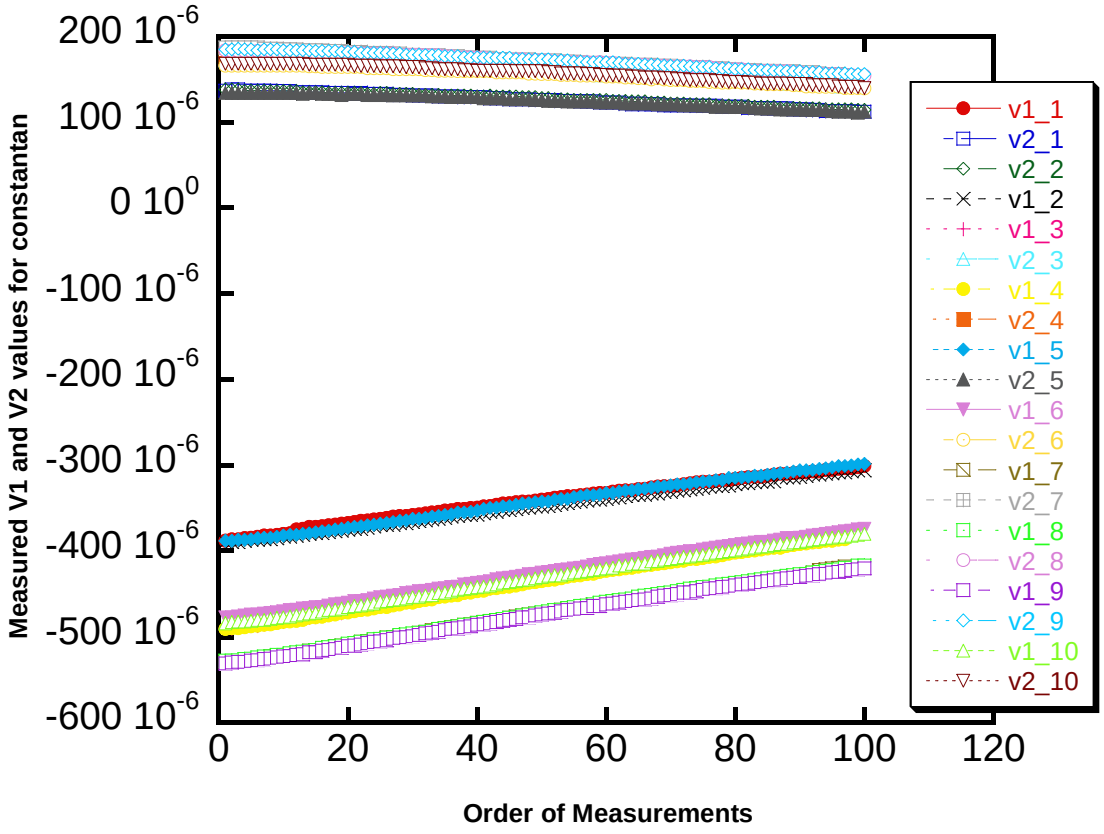

Figure 4.11: Measured values of V_1 and V_2 for constantan.

These two measurements show the major source of errors using this technique. For samples with thermopower values near those of constantan and copper, there was an error

created by an offset in voltage. This error is less pronounced for constantan due to the fact that the offset did not greatly affect the magnitude of V_1 which is used to determine the thermopower as ($V_1/V_2 - V_1$). For samples with thermopower values closer to copper the offset has a large effect in the magnitude of V_1 which accounts for the large errors.

In the previous examples the thermopower of the samples were either equal copper or constantan where either V_1, or V_2 was expected to equal zero respectively. To investigate a reference material with a thermopower between that of copper and constantan, a nickel sample was prepared. Nickel has a room temperature thermopower of -19.5μV/K [20]; the expected values of V_1 and V_2 for nickel are shown in Figure 4.12.

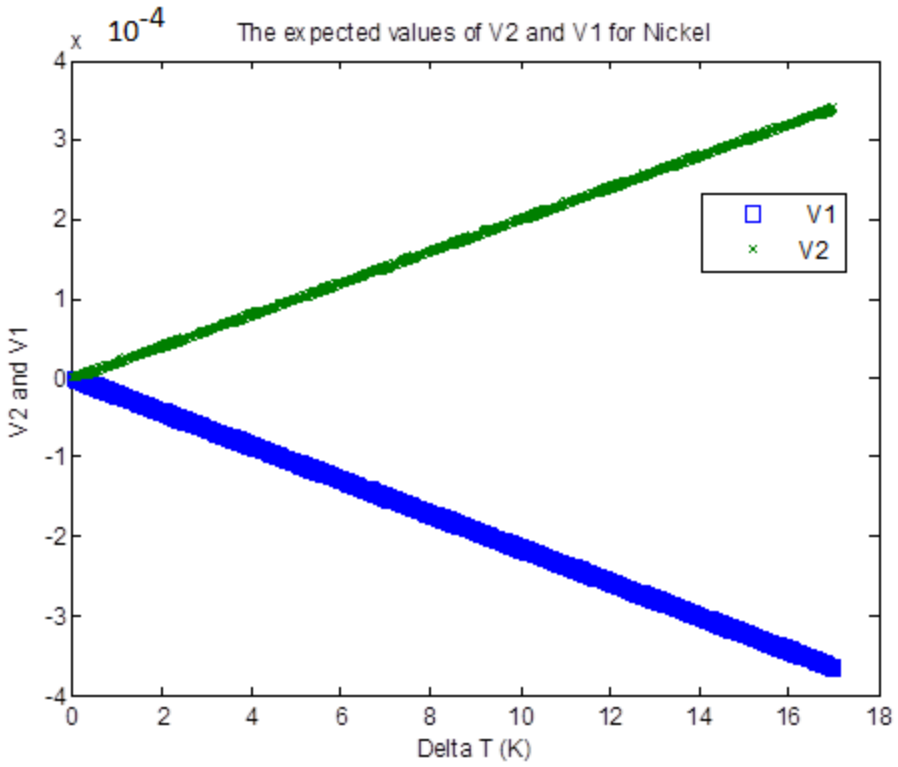

Figure 4.12: Expected values of V_1 and V_2 for nickel.

Figure 4.12 shows the values of V_1 and V_2 diverge as the temperature gradient gets larger.

Measurements of a nickel sample showed the values of V_1 and V_2 were equal in magnitude.

Unlike the other samples where one slope of a particular voltage grew larger than the other, for nickel which has a room temperature thermopower value approximately halfway between copper and constantan the values of V_1 and V_2 are almost equal in magnitude and their magnitudes increasing equally to each other with a rising temperature gradient. This makes it possible for equation 4.1 to be used to calculate an accurate temperature gradient for samples with thermopower values in a similar range. From the measured values of nickel there were no noticeable offsets from the expected voltage values (shown in Figure 4.13).

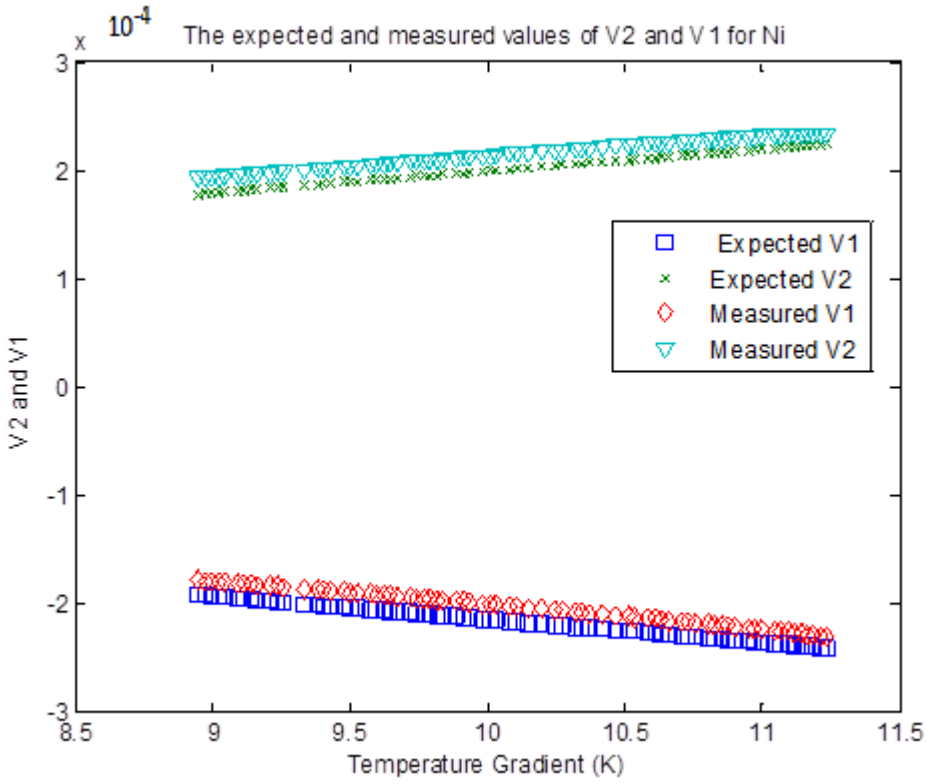

Figure 4.13: Expected and measured values of V_1 and V_2 for nickel.

Figure 4.14 shows ten measurements of the thermopower of nickel ranging from -24.763μV/K to -22.0445μV/K with an average thermopower value of -23.2μV/K.

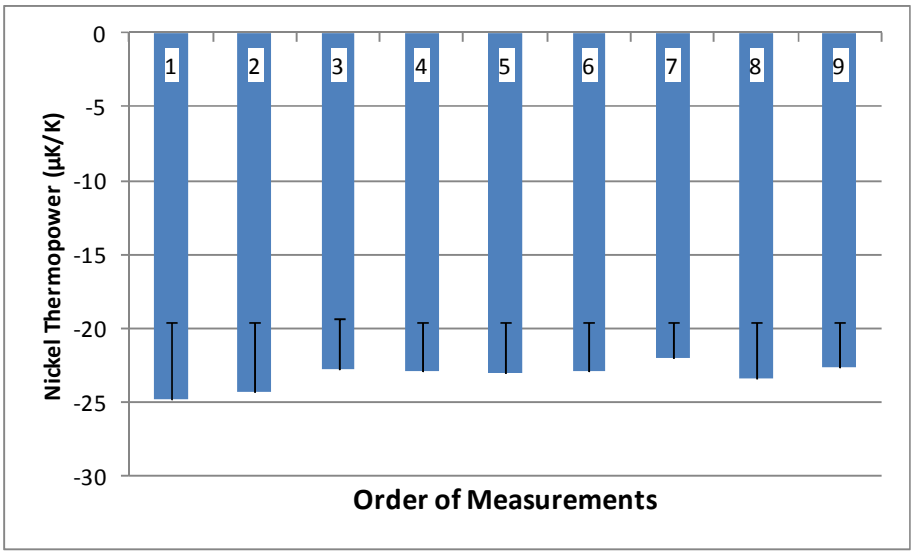

Figure 4.14: Nickel thermopower data.

The corresponding V_1 and V_2 measurements for these values are shown in Figure 4.15.

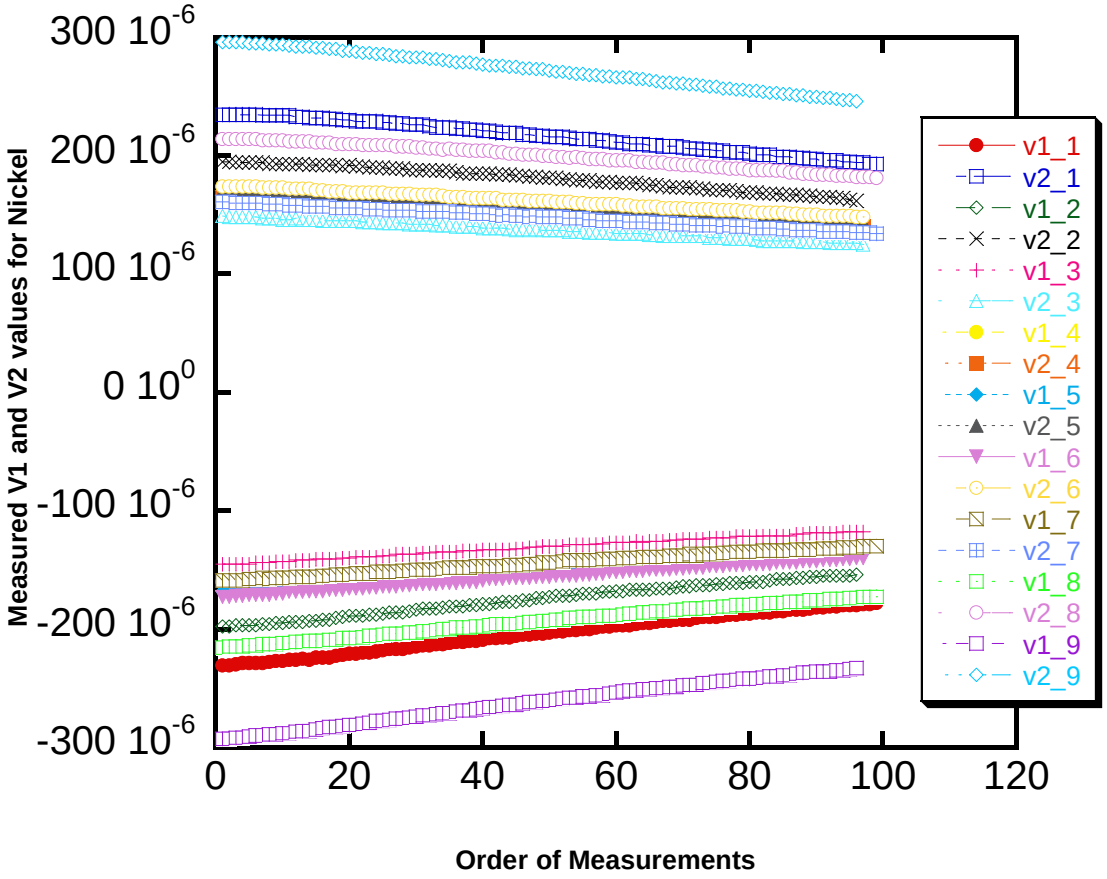

Figure 4.15: Measured values of V_1 and V_2 for nickel

In conclusion while analyzing the voltage measurements used to calculate the thermopower of reference samples, the source of errors between measured and expected results was found to be an offset in the magnitude of the voltages. This offset was largest for constantan and copper. The error was greatest in samples with relatively small thermopower due to the fact that V_1 was greatly shifted from its expected value, causing a greater error in the $V_1/(V_2 - V_1)$ slope which is used to calculate the thermopower of a sample. These measurements also showed that $V_2 - V_1$ is a reliable method of measuring the temperature gradient across the samples.

Chapter 5: Measurements of segmented thermoelectric bulk material composed of Bi_2Te_3 and LAST/LASTT.

5.1 Introduction:

Devices such as thermoelectric generators operate over large temperature gradients, but the materials used to create these devices have limited efficiency due to the fact that their peak *ZT* is restricted to a small temperature range. To maximize the average *ZT* over the hot to cold side temperature range, segmentation of the thermoelectric legs can be used. In this case, two or more n-type materials are joined to form the n-type legs, and likewise two or more p-type materials are joined to form the p-type legs. Such a configuration allows for larger temperature gradients by combining lower melting point materials with higher melting point materials. The larger hot to cold side temperature gradients also improves the efficiency of thermoelectric generators since they are Carnot efficiency limited. For smaller temperature gradients segmentation based on a single material system with minor compositional variation (doping, alloying) can also be used [21].

In this chapter segmented legs for thermoelectric devices using n and p-type Bi_2Te_3 and LAST (lead-antimony-silver-tellurium) and LASTT (lead-antimony-silver-tin-tellurium) are presented. Bi_2Te_3 is a well known thermoelectric material which has a peak *ZT* of ~1.0 at room temperature. LAST and LASTT are n-type and p-type materials respectively with peak *ZT* values near 700 K. Each material was in powder form and PECS processing was used to form the segmented samples. The following sections will document this process and the measurements taken by the room temperature thermopower scanning probe of these samples.

5.2 PECS

Both samples were made using Pulsed Electric Current Sintering (PECS). Also known as Spark Plasma Sintering, this method uses a pulsed DC current to heat the powder sample by Joule heating. High heating and cooling rates can be used since this method allows a direct way of heating. This allows for densification over grain growth promoting diffusion mechanisms, maintaining the intrinsic properties of nano-powders in their fully dense products. Temperature gradients inside the sample should be minimized in order to permit homogenous sintering behavior [22].

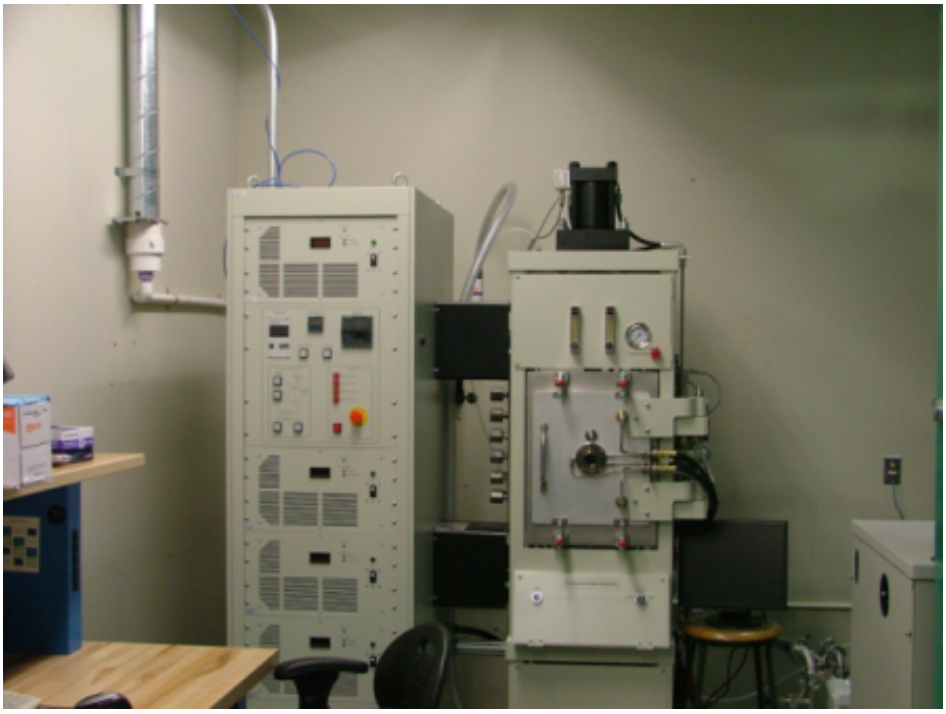

Figure 5.1: PECS system at MSU.

5.3 LAST/LASTT

LAST is an n-type semiconductor with a chemical formula of $AgPb_mSbTe_{2+m,}$ while LASTT is a p-type semiconductor with a chemical formula of $Ag(Pb_{1-x}Sn_x)_mSbTe_{2+m}$ [23]. In

recent years LAST was considered a material of interest because of its high *ZT* value compared to other TE materials. LAST exhibits desirable properties such as isotropic morphology, high crystal symmetry, low thermal conductivity and controllable carrier concentration [24]. LASTT has been reported to exhibit high performance p-type TE properties, such as a *ZT*~1.45 at 630 K. A sample with the composition $Ag_{0.5}Pb_6Sn_2Sb_{0.2}Te_{10}$ had a reported electrical conductivity of 1000 S/cm and a thermopower of roughly 50μV/K at room temperature [25].

5.3.1 Preparation of LAST/LASTT

Due to their desirable properties at high temperatures, LAST and LASTT were used as a hot side material for the n and p-type segmented samples. Each material was in powder form before PECS processing. Approximately 3g of LAST and LASTT powder was used to fill a 12.7mm diameter graphite die. They were placed separately inside the PECS system and processed in an argon environment at a maximum temperature of 550°C and pressure of 60MPa. The following profile was used during the PECS process:

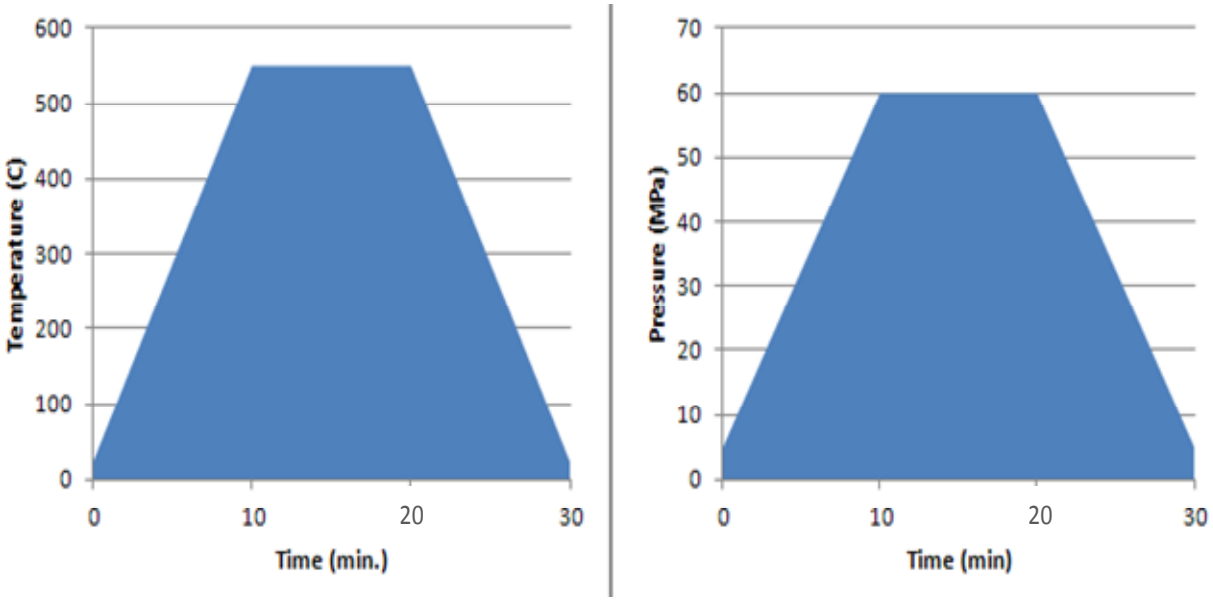

Figure 5.2: Temperature and pressure profiles for LAST/LASTT PECS processing.

Figure 5.3 shows the finished sample after PECS processing. The LASTT and LAST billets were approximately 2.5mm thick after pressing.

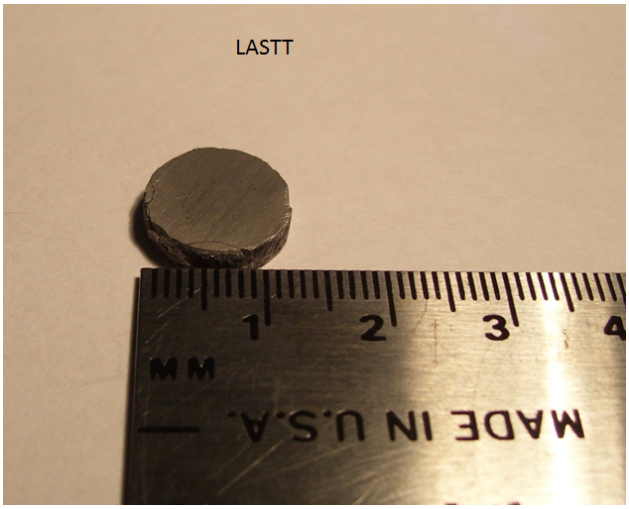

Figure 5.3: LASTT coin after PECS processing.

5.4 Preparation of Bi_2Te_3

Bi_2Te_3 was used as the material for the cold side of the segmented sample. The preparation process began with 5mm × 5mm × 2mm cubes of n and p-type Bi_2Te_3 from the Tellurex Corporation. The cubes were crushed into powders using a mechanical mortar and pestle, and 3g for both the n-type and p-type were prepared by sieving through a 53µm sieve. The powder was placed in a 12.7mm diameter graphite die with the already PECS processed LAST/LASTT samples inside, as illustrated in Figure 5.4.

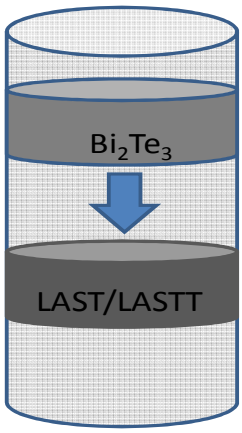

Figure 5.4: Bi_2Te_3 powder placed on top of PECS processed LAST/LASTT material.

The Bi_2Te_3 powder was processed at a gradually increase of temperature to a maximum temperature of 430°C. The processing began with an initial increase in temperature from room temperature to 110°C at a rate of 40°C/min, followed by a 10 minute hold at 110°C. Then the temperature was increased to 410°C at a rate of 60°C/min. Finally at a rate of 5°C/min the temperature was increased to 430°C. Throughout this process the pressure stayed constant at 40MPa. At 430°C, the pressure was increased to 50 MPa and the temperature remained at 430°C for a period of 20 minutes. At the end of that twenty minute period, the system gradually cooled down using the previously stated process in reverse, from 430°C to room temperature. Figure 5.5 shows the merged Bi_2Te_3 and LAST material after PECS processing.

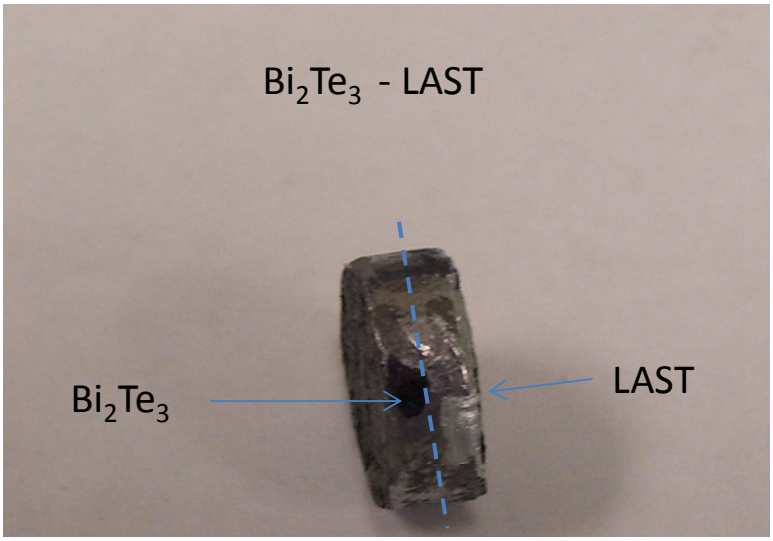

Figure 5.5: Finished PECS processed Bi_2Te_3 and LAST.

After excess graphite material was polished off the surface, the samples were cut into two rectangular pieces. Figure 5.6 is an image from an optical microscope, showing a distinction between the two materials after processing.

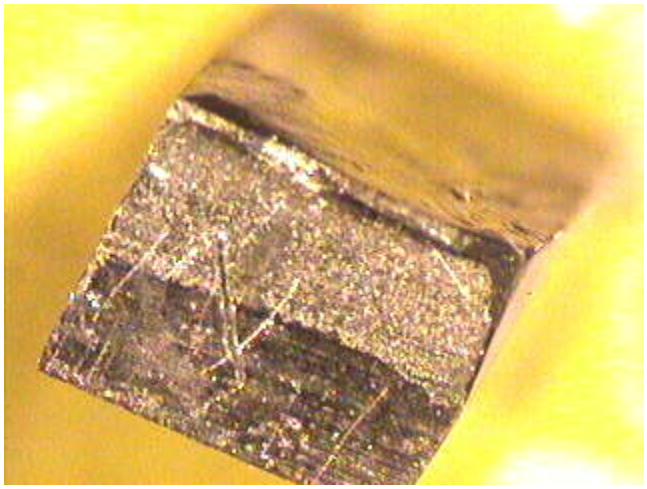

Figure 5.6: Optical microscope image of Bi_2Te_3 and LAST surface after processing.

5.5 Scanning Probe Measurements

The thermopower scanning probes was used to take several scans of the two segmented leg samples. For the n-type Bi_2Te_3/LAST material the surface scan distance was 5mm across in the Y-direction. The system was programmed to measure in 0.5mm increments. After a completed scan, the system moved a distance on 1mm in the X direction and another scan initiated in the Y direction.

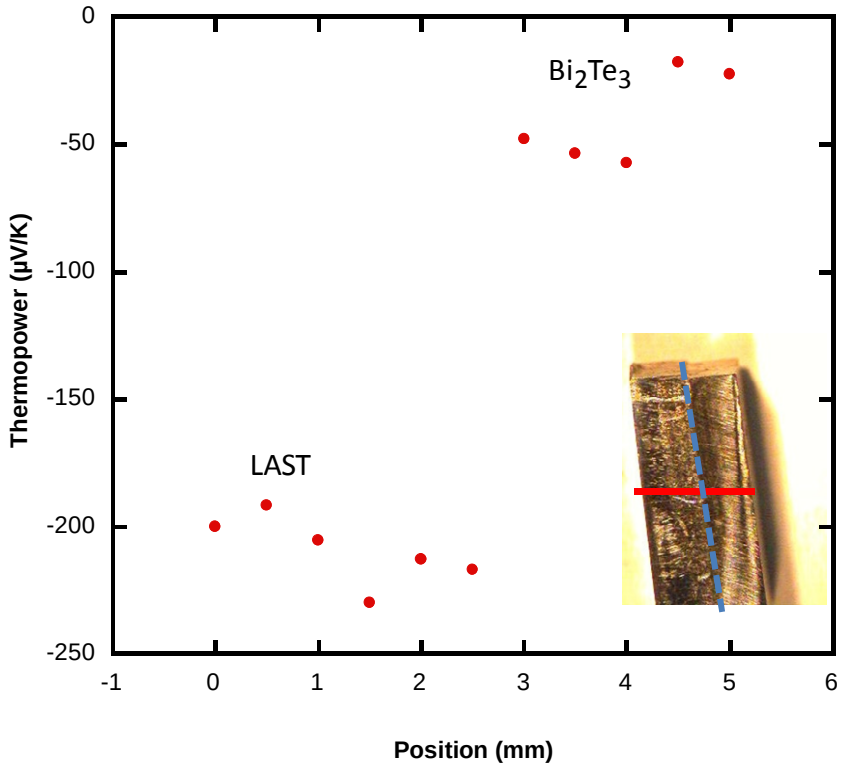

Figure 5.7: LAST/Bi_2Te_3 scan across the center of the sample (as shown in the inset).

Figure 5.7 shows the LAST material has a high thermopower (approximately -200µV/K). The thermopower scan shows a clear demarcation between the LAST material and the Bi_2Te_3 based material at approximately 2.8mm. The measurements also show a significantly lower

thermopower for the Bi_2Te_3 sample than expected based on the results from Figure 4.1. The solid Bi_2Te_3 cubes used to create the powder for this sample had a thermopower slightly less than -200μV/K, this scan shows that this thermopower dropped to ~-50μV/K. The cause of this can be the Bi_2Te_3 cubes were not properly crushed into powder form. Also this can be a side effect of using previously processed material in this procedure. This was the case for both n and p-type Bi_2Te_3material, as will be shown in the following figures.

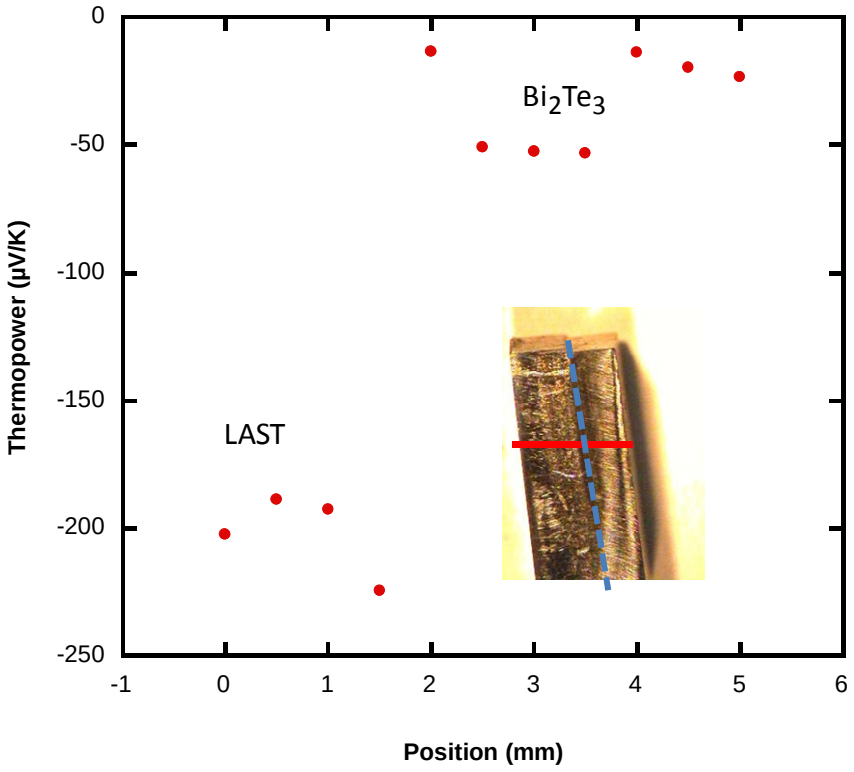

Figure 5.8: LAST/Bi_2Te_3 scan at 1mm behind the first scan at the center of the sample.

Figure 5.8 shows the second scan 1mm behind the origin. This scan shows agreement in measurements with the scan at the origin for the first 2mm, but between 2mm and 2.5 mm there was a dramatic drop in thermopower values. This is possibly due to a mixture in materials during

the fusion of the two different alloys. The two measurements also shows towards the outer edges of the Bi_2Te_3 material, the scans show a consistent drop in thermopower, which can mean the sample becomes more metallic at this point. Electro-dispersive X-ray spectroscopy (EDS) analysis of the samples surface was done to verify which materials were in each half of the sample. Table 5.1 shows area 1 is predominantly Bi and Te. While the analysis for area two shows the two prominent elements were Te and Pb.

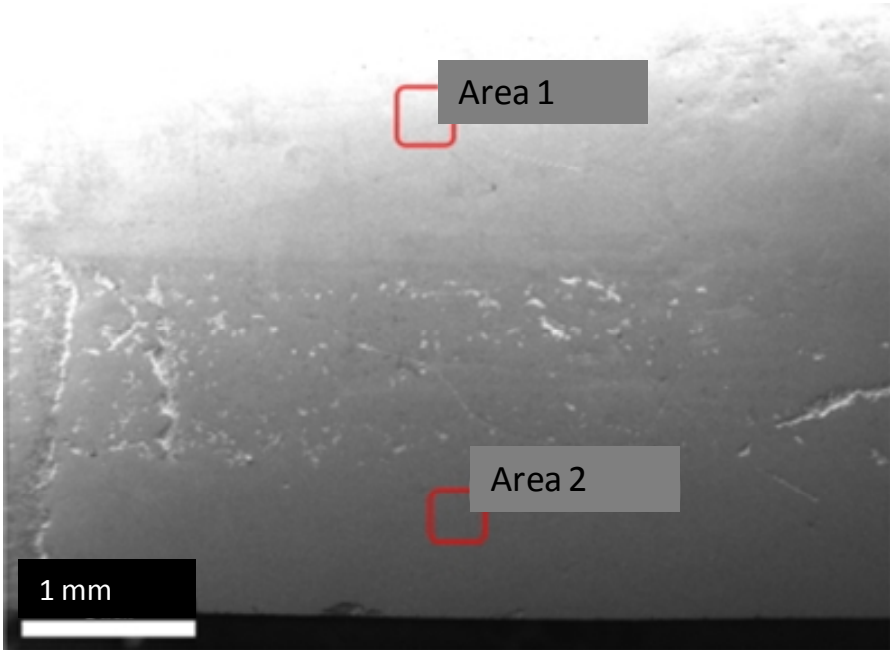

Figure 5.9: SEM surface image of LAST/Bi_2Te_3 sample.

Table 5.1: EDS analysis of area 1 in SEM image of LAST/Bi_2Te_3 sample.

Element	Weight %	Atomic %
BiM	47.11	34.85
SbL	0.56	0.71
TeL	50.97	61.76
SeK	1.36	2.67

Table 5.2: EDS analysis of area 2 in SEM image of LAST/Bi_2Te_3 sample.

Element	Weight %	Atomic %
PbM	50.62	35.45
AgL	4.76	6.4
SbL	2.59	3.08
TeL	40.62	46.18

For the p-type Bi_2Te_3/LASTT material the surface scan distance was 3mm as shown in Figure 5.10. The system scanned at 0.5mm increments, when this scan was complete the system moved a distance on 1mm in the X direction and another scan taken. The measurements for LASTT were between 50µV/K and 65µV/K, which is comparable to the values presented in literature [26]. Similar to the n-type Bi_2Te_3 in the LAST/ Bi_2Te_3 sample, the thermopower of the p-type Bi_2Te_3 material was significantly lower than the expected ~200µV/K. In this case the thermopower values for the p-type Bi_2Te_3 material were between 60-70µV/K. Unlike the

LAST/Bi_2Te_3 sample, in this LASTT/Bi_2Te_3 sample there are no clear distinctions between the two materials as shown in Figures 5.10 and 5.11.

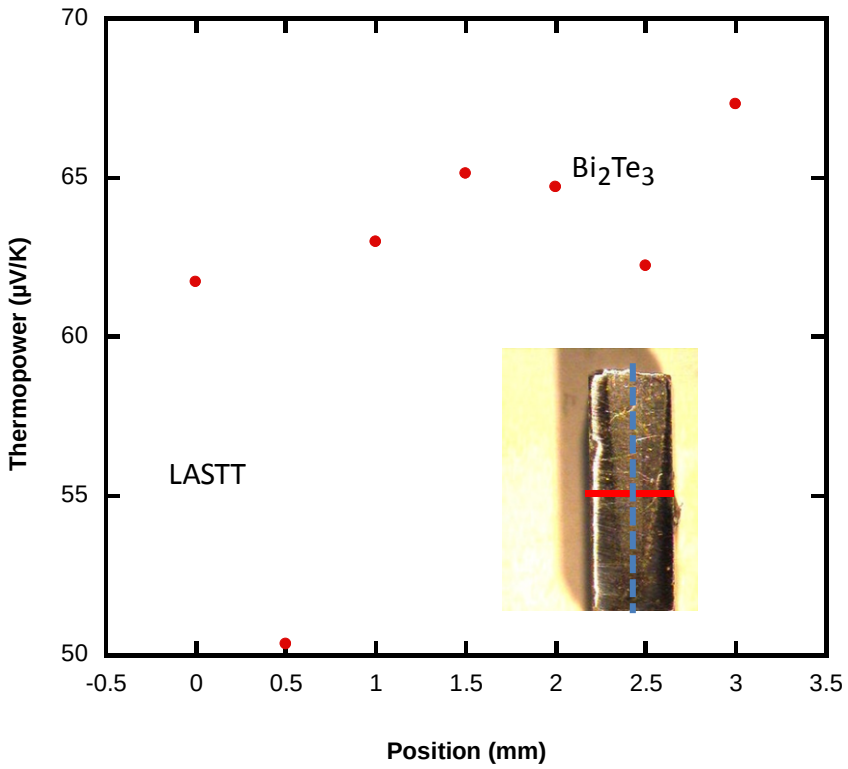

Figure 5.10: LASTT/Bi_2Te_3 scan across the center of the sample.

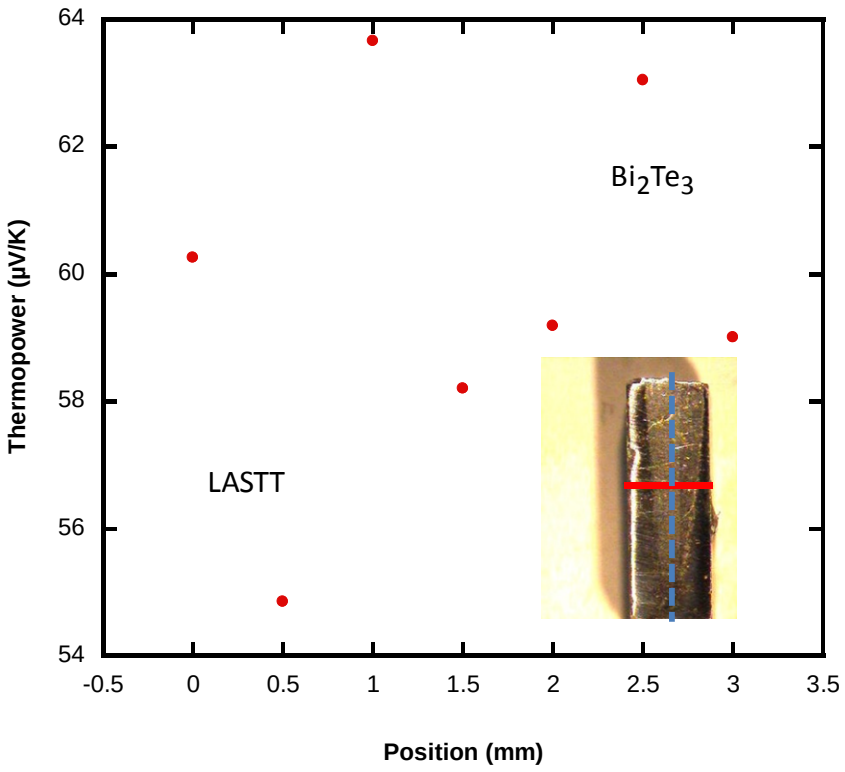

Figure 5.11: LASTT/Bi_2Te_3 scan at 1mm behind the first scan.

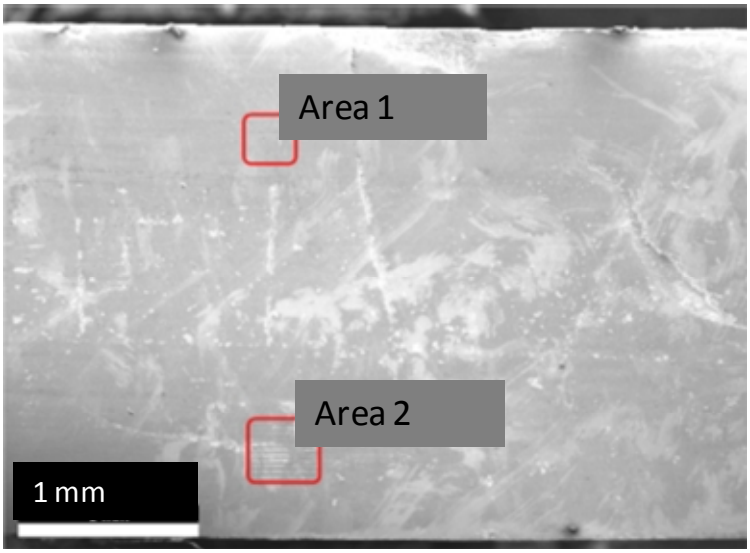

Figure 5.12: SEM surface image of LASTT/Bi_2Te_3 sample.

Table 5.3: EDS analysis of area 1 in SEM image of LASTT/Bi_2Te_3 sample.

Element	Weight %	Atomic %
PbM	25.23	15.11
AgL	1.91	2.2
SnL	19.69	20.58
SbL	2.62	2.67
TeL	47.99	46.66

Table 5.4: EDS analysis of area 2 in SEM image of LASTT/Bi_2Te_3 sample.

Element	Weight %	Atomic %
BiM	12.07	7.18
SbL	27.56	28.15
TeL	56.02	54.6
SeK	3.23	5.1

Using measurements of the TE materials composed of n-type LAST and Bi_2TE_3 and the p-type LASTT and Bi_2TE_3, the thermopower scanning probe showed a roll this type of system can have in TE research. For the n-type LAST and Bi_2TE_3 material, the results showed relative agreement between the expected and measured results for the LAST material. The measured

thermopower values of LAST were higher in magnitude than their expected values; it is suspected this is due to increased doping. In the EDS results shown in Table 5.2, Ag and Sb show a 2:1 relationship instead of a 0.8:1 relationship. This might be the cause of the increase in magnitude for the thermopower of the LAST material. For the n-type Bi_2TE_3 material the measured thermopower values were drastically lower than their expected value, the method of which this material was processed is suspected to be the reason behind the drop in thermopower values. For the p-type LASTT and Bi_2TE_3 material, the LASTT material showed close agreement between measured and expected thermopower values. The p-type Bi_2TE_3 material in this sample also showed a drastic drop in magnitude between measured and expected values, similar to the n-type Bi_2TE_3 material. These initial measurements showed the potential this system has in expanding future TE research, with greater improvement to automation and resolution future generations of this system will be able to provide better insight into this type of research.

Chapter 6: Conclusion and Future Work

6.1 Conclusions

A new scanning probe system has been presented for better characterization of thermoelectric materials. The system allows for characterization of the surface of a sample in two dimensions. Using the Seebeck coefficient, the degree of homogeneity of a sample can be attained by taking measurements from point to point across the surface of a sample. This information gives researches greater insight into the composition of specific samples, where other measurement methods only allow for single thermopower measurements of homogeneous samples. Reference measurements were taken to show the system operates as desired for high thermopower samples. The system was used in a study of segmented thermoelectric materials composed of n and p-type Bi_2Te_3 and LAST/LASTT to show the systems value in future research of inhomogeneous samples.

6.2 Future Work

From the onset of this project the intent was to build a scanning probe system that would be able to measure thermopower at room temperature and create a two dimensional characterization of a sample. As a prototype the system was successfully built and programmed to work as it was originally intended. Over the course of the research various issues with the design and programming developed that showed areas that can be improved in the overall design of the system. Moving forward in order to build on the work presented in this thesis and improve the capabilities of the system the following improvements are advised:

1. Motors – The three stepper motors used by the system required at least 12V- 2.5A to work properly. These motors give off a considerable amount of heat after being on for a short amount of time. This presents a few problems that will have to be addressed. The

system was not tested for a prolonged period of time because it was unclear what kind of damage this amount of heat would do to the motors and circuitry. Also this heat is transported through the motor mounts into the translation stage. Since these measurements are dependent on the temperature around the sample remaining constant, any ambient heat given off by the stage and the motors can cause inaccuracies in the measurements. If the system is to be operational for a prolonged period of time, the amount of heat given off by the motors has to be addressed.

2. Probe - Another issue that needs to be addressed is the resolution of the probe. The true resolution of the probe was not quantified in these initial tests of the system. Moving forward a better understanding of the probes resolution can lead to greater surface characterization. One area that can be studied is the interaction at the interface of thermoelectric materials and metal contacts in devices. With a finer resolution the thermopower scanning probe would be able to show the effects of bonding metals and thermoelectric material. Thermoelectric devices use metals such as stainless steel to separate n and p-type thermoelectric material and to act as electrical connections. This system can be used to study any doping that occurs to the thermoelectric materials when they are bonded with the metal interconnects.

Appendix

Appendix A

Table A-1: Material composition of thermocouples and their temperature ranges [26]

Type	Positive element	Negative element	Temperature Range (C)
B	Platinum(70%),Rhodium(30%)	Platinum(94%),Rhodium(6%)	800 to 1700
E	Nickel(90%), Chromium(10%)	Constantan: Nickel(55%), Copper(45%)	0 to 900
J	Iron	Constantan: Nickel(55%), Copper(45%)	0 to 750
K	Nickel(90%), Chromium(10%)	Ni(95%), Al(2%), Mn(2%),Si(1%)	0 to 1250
N	Ni(84.4%), Cr(14.2%),Si(1.4%)	Ni(95%), Si(4.4%),Mn(0.15%)	500 to 1000
R	Platinum(87%),Rhodium(13%)	Platinum	0 to 1450
S	Platinum(90%),Rhodium(10%)	Platinum	0 to 1450
T	Copper	Constantan: Nickel(55%), Copper(45%)	0 to 350

Table A-2: Coefficients of the calibration equation for voltage as a function of temperature (eq.2.20) for type-T thermocouples [26]

	0°C ≤ T ≤ 400°C
b0	0
b1	3.8748106364E-02
b2	3.329222788E-05
b3	2.0618243404E-07
b4	-2.1882256846E-09
b5	1.0996880928E-11
b6	-3.0815758772E-14
b7	4.5479135290E-17
b8	-2.7512901673E-20

Table A-3: Coefficients of the calibration equation for temperature as a function of voltage (eq.2.21) for type-T thermocouples [26]

	$0mV \leq E_{0j} \leq 20.872mV$
c0	0
c1	2.5928E+01
c2	-7.602961E-01
c3	4.637791E-02
c4	-2.165394E-03
c5	6.048144E-05
c6	-7.293422E-07
c7	0

Bibliography

Bibliography

[1] Snyder, G. Jeffrey, and Eric S. Toberer. "Complex Thermoelectric Materials" *Nature Materials* 7.2 (2008): 105-14.

[2] Mahan, G. D., and L. M. Woods. "Multilayer Thermionic Refrigeration." *Physical Review Letters* 80.18 (1998): 4016-019.

[3] S. Loo, *36-Sample Measurement System For Doping and Alloying Trends in New Thermoelectric Material*s, Master's Thesis, Michigan State University, 2000

[4] Kasap, Safa, *Thermoelectric effect in metals: Thermocouples*, http://kasap3.usask.ca/samples/Thermoelectric-Seebeck.pdf

[5] Emin, David. "Seebeck Effect." *Wiley Encyclopedia of Electrical and Electronics Engineering*. John Wiley & Sons, 2001. Online.

[6] Bardas, Athanassios. "Peltier Effect." *Wiley Encyclopedia of Electrical and Electronics Engineering*. John Wiley & Sons, 2001. Online.

[7] Tegeder, V., and C. Tegeder."Thermoelectricity." *Ullmann's Encyclopedia of Industrial Chemistry*.Wiley-VCH Verlag GmbH &KGaA, 2000.Online.

[8] Razeghi, Manijeh. *Fundamentals of Solid State Engineering*. New York: Springer, 2009.

[9] G. Mahan, "Good Thermoelectrics", Solid State Physics, vol 5.1, 1998.

[10] Gerald Recktenwald (2010), *Conversion of Thermocouple Voltage to Temperature*, [Online]. Available: web.cecs.pdx.edu/~gerry/epub/pdf/thermocouple.pdf

[11] Cowles, L E J., and L. A. Dauncey. "Apparatus for the Rapid Scanning of the Seebeck Coefficient of Semiconductors." *Journal of Scientific Instruments* 39.1 (1962): 16-18. Print.

[12] Goldsmid, H. J. (1986). "A simple technique for determining the Seebeck coefficient of thermoelectric materials". *Journal of Physics E Scientific Instruments*, *19*(11), 921.

[13] Platzek, D., G. Karpinski, CestmirDrasar, and Eckhard Müller. "Seebeck Scanning Microprobe for Thermoelectric FGM." *Materials Science Forum* 492-493 (2005): 587-92.

[14] "UCN5804B Datasheet PdfDatenblatt - Allegro MicroSystems - BiMOS II UNIPOLAR STEPPER-MOTOR TRANSLATOR/DRIVER ::: ALLDATASHEET :."*ALLDATASHEET.COM - Datasheet Search Site, Datasheet Search Site for Electronic Components and Semiconductors and Other Semiconductors.* Web. 21 July 2011. http://www.alldatasheet.com/datasheet-pdf/pdf/55138/ALLEGRO/UCN5804B.html?.

[15] *NI USB-6501 Low-Cost USB Digital I/O Device*. National Instruments. Web. 21 July 2011. <http://sine.ni.com/ds/app/doc/p/id/ds-135/lang/en>.

[16] A. Downey, *Advancing Thermoelectric Research With New Measurement Systems and Thermoelectric Modeling For AC Electrical Measurements*, Ph.D, Michigan State University, 2006

[17] Lowhorn,N.; Wong-Ng, W. K.; Zhang, W.; Lu, J.; Otani, M.; Thomas, E. L.; Green,M.L.; Tran, T. "Round-Robin Studies of Two Potential Seebeck Coefficient Standard Reference Materials", *Applied Physics A-Materials Science & Processing*, 94(2009):231 – 234.

[18] Z.Q.J. Lu, N.D. Lowborn, W. Wong-Ng, W. Zhang, E.L. Thomas, M. Otani, M.L. Green, T.N. Tran, C. Caylor, N.R. Dilley, A. Downey, B. Edwards, N. Elsner, S. Ghamaty, T. Hogan, Q. Jie, Q. Li, J. Martin, G. Nolas, H. Obara, J. Sharp, R. Venkatasubramanian, R. Willigan, J. Yang, T. Tritt"Statistical Analysis of a Round-Robin Measurement Survey of Two Candidate Materials for a Seebeck Coefficient Standard Reference Material" *J. Res. Natl. Inst. Stand. Technol.* 114.1(2009): 37.

[19] Roberts, R. B. "The Absolute Scale of Thermoelectricity II." *Philosophical Magazine Part B*43.6 (1981): 1125-135.

[20] Rosa, Aldo Vieira. *Fundamentals of renewable energy processes.* 2nd ed. Amsterdam: Elsevier Academic Press, 2009.

[21] Müller, E. "Functionally Graded Materials for Sensor and Energy Applications." *Materials Science and Engineering A* 362.1-2 (2003): 17-39.

[22] Pulsed Electric Current Sintering (PECS) or Spark Plasma Sintering (SPS)." KatholiekeUniversiteit Leuven, 13 Aug. 2009. Web. 21 July 2011. <http://sirius.mtm.kuleuven.be/Research/C2/pulsed_electric_current_sintering/index.html>.

[23] Bradley Hall, *Powder processing, powder characterization, and mechanical properties of LAST and LASTT thermoelectric materials*, Master's Thesis, Michigan State University, 2008.

[24] Hsu, K. F. "Cubic AgPbmSbTe2+m: Bulk Thermoelectric Materials with High Figure of Merit." *Science* 303.5659 (2004): 818-21.

[25] Androulakis, J., K.F. Hsu, R. Pcionek, H. Kong, C. Uher, J.J. D'Angelo, A. Downey, T. Hogan, and M.G. Kanatzidis. "Nanostructuring and High Thermoelectric Efficiency in P-Type Ag(Pb1–ySny)mSbTe2+m." *Advanced Materials* 18.9 (2006): 1170-173.

[26] American Society for Testing and Materials, *A Manual on the Use of Thermocouples in Temperature Measurements.* ASTM, Philadelphia, New York, fourth edition, 1993.